



Review Article

Recent advances and new research trends in Sb₂S₃ thin film based solar cellsMohaiyadeen Aliyar Farhana ^a, Arumukham Manjeevan ^b, Jayasundera Bandara ^{a, *}^a National Institute of Fundamental Studies, Hantana Road, CP 20000, Kandy, Sri Lanka^b Department of Chemistry, Faculty of Science, University of Jaffna, Sri Lanka

ARTICLE INFO

Article history:

Received 9 August 2022

Received in revised form

1 November 2022

Accepted 6 January 2023

Available online 11 January 2023

Keywords:

Sb₂S₃ thin-film

Structure

Morphology

Photovoltaic performances

Thin-film solar cell

ABSTRACT

Although many environmentally friendly and non-toxic materials have been investigated for photovoltaic conversion (PVC) applications, Sb₂S₃ is the material of choice as an absorber in thin-film solar cells due to its broad-band optical response and excellent electrical properties. Though an Sb₂S₃ thin-film was predicted to have a 28% efficiency, the reported efficiency of 7% is significantly lower than the theoretically predicted efficiency and less competitive compared to other similar thin-film solar cells. This review investigates how structural and morphological changes in Sb₂S₃ thin films contribute to the current state of Sb₂S₃ solar cell development to understand and improve current device performance. We first discuss the fundamental structure and properties of Sb₂S₃ and then show how morphology and structural changes in Sb₂S₃ thin films produced using various fabrication techniques and conditions affect solar cell performance. This research includes several significant recent developments and current research trends that will pave the way for future improvements in the performance of Sb₂S₃-based photovoltaic solar cells.

© 2023 Vietnam National University, Hanoi. Published by Elsevier B.V. This is an open access article under the CC BY license (<http://creativecommons.org/licenses/by/4.0/>).

1. Introduction

As the world's population continues to grow exponentially, so makes the energy demand. The majority of today's energy demand is met by fossil fuels, which are in short supply and pollute the environment by emitting gases such as CO₂, SO₂, NO₂, CO, etc. [1] The total global energy demand is gradually increasing, with a 48% increase expected in 2040 compared to 2012 [2]. As a result, it is critical to identify and exploit environmentally clean and renewable energy sources that can replace conventional energy resources. Renewable energy consumption grows faster than other energy sources, increasing by an average of 2.6% per year. There are numerous renewable energy sources available, including wind, hydro, bio, and solar energy, where 1 h of solar energy strikes the earth is enough to meet the world's annual energy consumption [2]. Therefore, solar photovoltaic (PV) technology has become popular, and more research is being conducted to improve the efficiency of light-harvesting ability and conversion of light energy into electrical energy. On a global scale, the annual installed power

capacity of solar PV is increasing at a faster rate [3]. Since solar PV has drawbacks such as higher fabrication/installation costs and lower power conversion efficiency (PCE), the research trend is primarily focused on synthesizing high-efficiency, low-cost light-harvesting earth-abundant materials with novel properties and a large number of studies have been conducted using chalcogenides thin-film solar cells [4–6]. Thin-film solar cells based on CdTe and CIGSSe, had power conversion efficiencies of 22.1 and 23.4%, respectively [7,8]. Thin-film solar cells based on CdTe and CIGSSe, on the other hand, are not cost-effective due to the use of highly sophisticated vacuum-based deposition methods in the fabrication of inorganic thin-film, such as vacuum evaporation and magnetron sputtering [5,7]. Due to their negative effects such as high fabrication costs, scarcity of tellurium (Te) and indium (In), and toxicity of Cd and Se, research on new materials such as Sb₂Se₃ and Sb₂S₃ is being focused [9,10]. Among them, Sb₂S₃ is an excellent candidate due to its unique properties, which include a high absorbance coefficient ($1.8 \times 10^5 \text{ cm}^{-1}$ at 450 nm), a 1.7 eV bandgap enabling absorbing visible regions of the spectrum, better stability in air and moisture, abundant raw materials, and availability of environmentally friendly fabrication processes [11–13]. Furthermore, the high crystalline quality films that can be synthesized at low temperatures due to Sb₂S₃'s low melting point (~550 °C) and the better

* Corresponding author.

E-mail addresses: aliyar.f@gmail.com (M.A. Farhana), manjeevan@gmail.com (A. Manjeevan), jayasundera.ba@nifs.ac.lk (J. Bandara).

Peer review under responsibility of Vietnam National University, Hanoi.

electron collection efficiency due to high electron diffusion length (290–900 nm) in Sb_2S_3 are some of the other favorable properties resulting in improved solar cell performance.

An Sb_2S_3 solar cell has a device structure similar to that of a dye-sensitized solar cell, which includes an electron transport layer, light-harvesting material, hole transport material, and a back contact (Fig. 1). When illuminated, the electron in the valence band of the Sb_2S_3 layer absorbs the light to form an excited state, and the excited electron is injected into the TiO_2 layer from the Sb_2S_3 absorber layer. Holes that are generated by the excitation of light are moved towards the p-type hole transport layer and collected by the back contact of the solar cell. The external connection between the photoanode and the back contact of the solar cell leads to follow the electron from the electron-rich photoanode to back contact through the external load resulting in electricity. The widely used electron transport materials are TiO_2 , ZnO , SnO_2 , and CdS [14–19] and mostly used hole transport materials are copper thiocyanate (CuSCN) [4,17], poly (3-hexylthiophene) (P3HT) [4,14,20], spiro-OMeTAD [21], NiO_x [22], V_2O_5 [23], gel polymer electrolyte [24] and liquid electrolyte [20,25]. As back contact, Au [12,14,26] or Ag [15,16,22] are commonly used. Recently, carbon was used as both HTM and back contact in Sb_2S_3 solar cells [27]. Fig. 2 shows the different stacking methods of Sb_2S_3 thin-film solar cells.

Recent reviews have reported on the advancement of Sb_2S_3 -based solar cells, and in those reviews, Sb_2S_3 -based photovoltaic devices focusing on semiconductor-sensitized and planar solar cells were comprehensively discussed, and preparation methods of antimony chalcogenide-based materials were briefly outlined [4,32]. The morphology of the Sb_2S_3 thin film, on the other hand, is one of the critical factors that contribute to device performance, which is dependent on the fabrication method. Different morphologies derived from the Sb_2S_3 fabrication method may pave the way for the development of optimized and highly efficient Sb_2S_3 -based solar cells and hence the morphology-dependent solar cell performance of Sb_2S_3 solar cells must be scrutinized. As a result, the focus of this review work is primarily on the effect of morphology and structure changes in Sb_2S_3 films on solar cell performance, which could be achieved through various fabrication methods and conditions on pristine Sb_2S_3 films.

Thin Sb_2S_3 films with different nanostructures such as smooth and textured have been fabricated by several methods such as chemical bath deposition (CBD) [15,18], spray pyrolysis [33–35], electro-deposition [36], thermal evaporation [37], atomic layer deposition (ALD) [14,38] and spin coating [22,39], etc. Table 1 summarizes the advantages and disadvantages of each Sb_2S_3 thin film deposition method.

As briefly discussed below, optimizing the structure and morphology of the light-harvesting Sb_2S_3 layer in solar cells by selecting the appropriate Sb_2S_3 film deposition technique improves device performance significantly. In solar cells, especially the charge carrier transport in planar solar cells is heavily influenced by absorber morphology. Large, compact grains are preferred to reduce grain boundary scattering and improve carrier transit across the film. The conventional CBD process and post-annealing approach do not typically produce large-grained compact films. Other methods and strategies to improve morphology have recently been employed. Sb_2S_3 planer thin-film solar cells have recently achieved 7.5% and 6.9% efficiency by sulfurizing with thioacetamide (TA) [11] and SbCl_3 treatment of the absorber layer, respectively [52]. When synthesized by spin-coating, Sung et al. discovered that rough TiO_2 , as opposed to flat TiO_2 , can improve the quality of Sb_2S_3 morphology and, as a result, device performance [53]. To obtain large grains, Wang et al. improved their solution-based deposition recipe [54]. As briefly discussed, optimizing the structure and morphology of the light-harvesting Sb_2S_3 layer in solar cells by selecting the appropriate Sb_2S_3 film deposition technique significantly improves device performance. This timely review is required to address the effect of morphology and structure changes in Sb_2S_3 films produced by thin Sb_2S_3 film fabrication methods, and thus on the performance of solar cells to address the development of promising Sb_2S_3 -based solar cells in the future.

2. Structure and morphology of Sb_2S_3

2.1. Basic structure and properties of Sb_2S_3

Antimony sulfide (Sb_2S_3) is a binary layered chalcogenide semiconductor of the A_2B_3 family ($\text{A} = \text{As}, \text{Sb}, \text{Bi}$ and $\text{B} = \text{S}, \text{Se}, \text{Te}$)

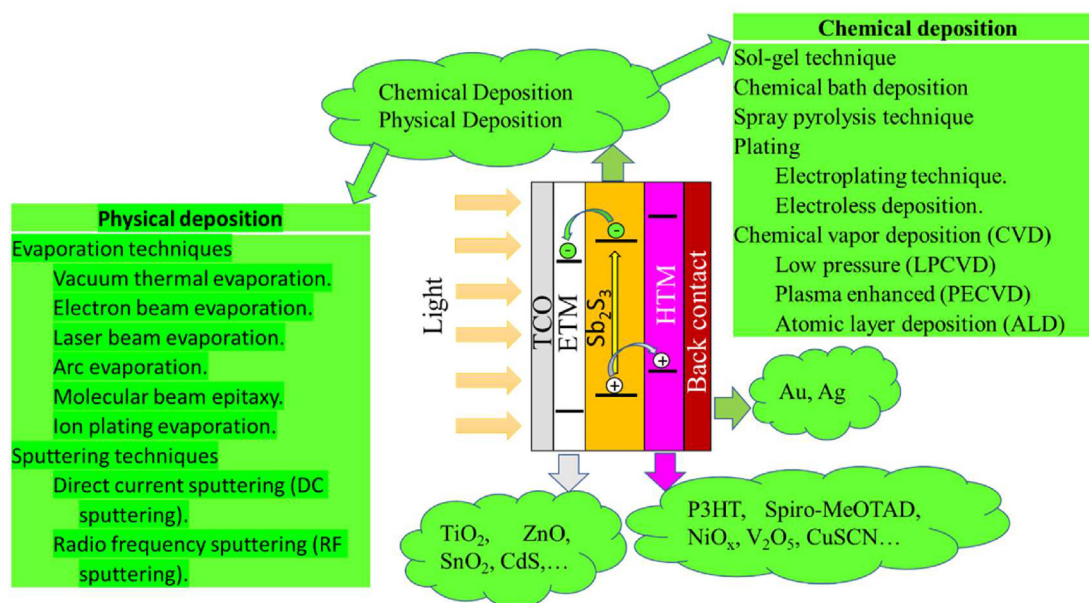


Fig. 1. Schematic diagram of solid-state nanocrystalline Sb_2S_3 thin-film solar cells and the deposition methods; ETM, HTM refer the electron transport materials and hole transport materials, respectively.

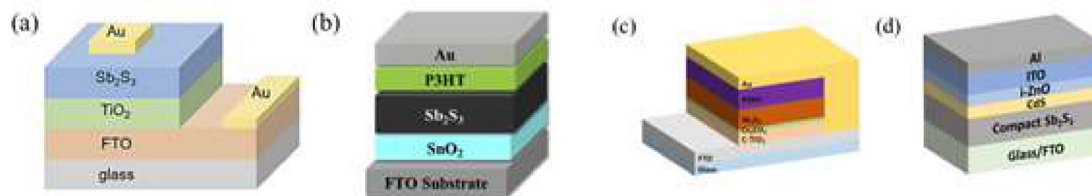


Fig. 2. Different stacking of Sb_2S_3 thin-film solar cells: (a) Glass/FTO/ TiO_2 / Sb_2S_3 /Au. Reproduced with permission [28], 2017, Elsevier. (b) Glass/FTO/ SnO_2 / Sb_2S_3 /P3HT/Au. Reproduced with permission [29], 2018, Elsevier. (c) Glass/FTO/compact TiO_2 / Cs_2CO_3 / Sb_2S_3 /P3HT/Au. Reproduced under terms of the CC-BY license [30], 2019, Springer. (d) Glass/FTO/Compact Sb_2S_3 /CdS/i-ZnO/ITO/Al. Reproduced with permission [31], 2019, Elsevier.

with high photosensitivity and thermoelectric properties [37,55]. The mineral form of Sb_2S_3 is known as stibnite and crystallizes at room conditions, and has an orthorhombic Pbnm space group crystal structure [4]. The calculated Sb_2S_3 lattice constants were $a = 11.3107 \text{ \AA}$, $b = 3.8363 \text{ \AA}$ and $c = 11.2285 \text{ \AA}$ and the density was 4.62 g cm^{-3} [55,56]. As shown in Fig. 3(a) and (b), the structure of infinite $(\text{Sb}_4\text{S}_6)_n$ chains is formed parallel to the needle axis (c-axis). In that, four minerals of the stibnite family crystallize in an orthorhombic structure consisting of parallel one-dimensional $(\text{A}_4\text{B}_6)_n$ ribbons (chains), with $\text{A} = \text{Sb}$, Bi , and $\text{B} = \text{S}$, Se [57]. At room pressure, Sb atoms are in two distinct positions, in each Sb is bonded with three and four S atoms with short and longer bonds respectively. These chains are linked to form crumpled (zigzag) sheets perpendicular to the a-axis or plane (100), and

these sheets (two per unit cell) are held together, which are held together to ensure perfect cleavage perpendicular to the b-axis. Antimony–sulfur (Sb–S) bonds are mainly covalent [56]. Fig. 3 (b) depicts the fundamental building blocks of the stibnite structure (Sb_2S_3 crystal), and the bond lengths within the ribbons differ due to different coordination by Sb and S. Because strong covalent bonding is dominant within the ribbon along the c axis, stibnite is less compressible along the c-axis compared to other directions, and electron concentration is high within the ribbons. However, atoms in ribbons and sheets are held together by very weak dangling bonds, particularly in a-axis [100] leading to single crystals cleaving easily in the direction perpendicular to the (100) plane. The orthorhombic Sb_2S_3 cubic crystal structure is strongly anisotropic due to the formation of infinite $(\text{Sb}_4\text{S}_6)_n$ ribbon-like

Table 1

Advantages, disadvantages of different types of deposition techniques and challenges faced in every deposition technique.

| Deposition technique | Advantages | Disadvantages | Challenges | Ref |
|----------------------|---|--|---|---------|
| ALD | High-quality films Uniform layers Precise thickness | Slow deposition Expensive | Additional annealing required | [38,40] |
| Spray pyrolysis | Easy to produce the doped films Low cost Thickness is controllable No restriction for the dimension of the sample Can be used in low temperatures (200–500 °C) Quiet compact and uniform film Different composition films can be produced | Precursor is a liquid solution | Thickness is not directly measured Possess surface roughness | [41–43] |
| CBD | Low cost Easy arrangements Can be done at room temperature | Slow Additional annealing required Film thickness is not directly measured | Impurities formation No linear growth Amorphous films | [44–46] |
| Electro-deposition | Quiet uniform film Growth controllable Low cost Low wastage of precursors Quiet uniform layer | Precursor is a liquid solution Amorphous films | Poor adhesion | [36] |
| Thermal evaporation | Simple arrangements Film rate controllable Compact and uniform layer Fast film growth Thickness measurable High-quality films | Instrument expensive Vacuum system required Relatively low throughput | Additional annealing required S loss due to high pressure | [47–50] |
| RF sputter | Possible to produce multilayers Good uniformity over a large area Fast film growth | Vacuum system required | High voltage could cause defects | [31,51] |
| Spin coating | Possible at room temperature Smooth morphology Smooth and compact film | Precursor solution is wasted | Poor crystallinity | [39,43] |
| | Simplest arrangement Thickness controllable | | Films with large areas produce non-uniformity Film thickness is not directly measured Additional annealing required | |

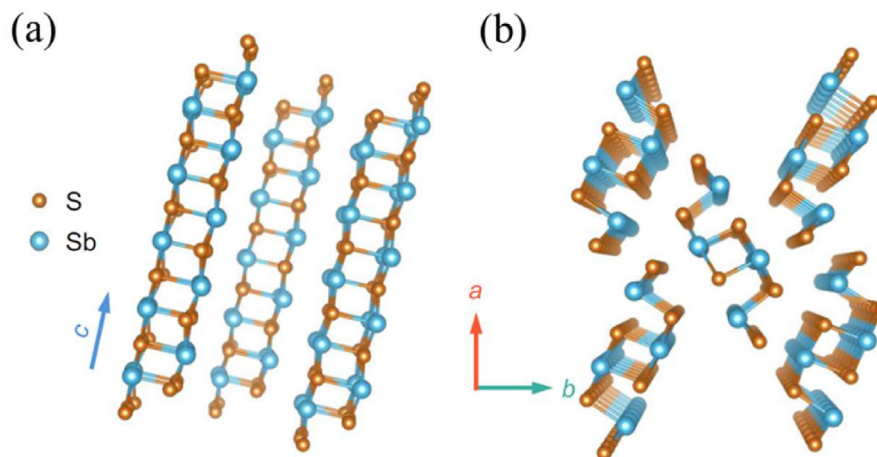


Fig. 3. Schematic diagram of quasi-1-dimensional structural Sb_2S_3 . Side view (a) and aero view, reproduced under terms of the CC-BY license [59], 2021, Nature. (b) Of $[\text{Sb}_4\text{S}_6]$ ribbons along the c axis. Reproduced under terms of the CC-BY license [59], 2021, Nature.

structures along the c -axis and very low dangling bonds at the surfaces perpendicular to the (001) plane, and thus one-dimensional (1D) ribbons exhibit highly anisotropic charge transport properties along with the ribbon structure, and solar cell performance is inextricably linked to the plane orientation [58].

The anisotropic nature of Sb_2S_3 and the distribution of bond lengths affect defect formation and energy levels in the bandgap [4]. The partial valence electron density is classified into three energy groups: low energy, medium energy, and high energy. Within each valence band group, the bands are highly dispersed along the ribbon direction [001] and less dispersed (flat) in other directions, such as [100] and [010]. These characters are highly dependent on the orientation of the path [60,61]. Since the band structure of Sb_2S_3 crystal highly resembles one another, Sb-5s and Sb-5p orbitals dominate the formation band structure more than S-3s and S-3p states. As a result, the experimental and theoretical bandgap values for Sb_2S_3 differ from the obtained values. The estimated bandgap of Sb_2S_3 is varied in the range of 1.56–2.25 eV [61]. The bandgap in amorphous Sb_2S_3 is indirect, whereas the bandgap in crystalline Sb_2S_3 is direct [62]. At room temperature, however, stibnite is a direct bandgap semiconductor. As the bandgap of Sb_2S_3 decreases with the increase of Sb_2S_3 crystallinity, the absorption of Sb_2S_3 increases with crystallinity [60]. Furthermore, the energy gaps vary with thickness. Relatively high absorption coefficient (α) has been experimentally determined in the order of 10^4 – 10^5 cm^{-1} in the visible range and near-IR spectral range [35]. The Sb_2S_3 films are non-degenerate and n -type at room temperature [63], and the conductivity of stibnite is 10^{-8} – 10^{-9} $\Omega^{-1}\text{cm}^{-1}$ at room temperature. Bohac and Kaufmann reported that in Sb_2S_3 crystal, the resistivity parallel to the ribbon direction is 100 times less than perpendicular [63]. In contrast, Roy et al. discovered that the conductivity along the ribbon is approximately 100 times greater than that of sheets [55]. Since the electrical conductivity of the films is temperature-dependent, attempts have been made to increase the conductivity by increasing the temperature of Sb_2S_3 films. At different temperatures, electrons in Sb_2S_3 jump from one site to another at the range of temperature 310–550 K, and as the temperature rises, the electrons become excited and free to move, resulting in increased electrical conductivity. In this review, we will discuss how Sb_2S_3 preparation methodologies influence the morphologies, structures, optoelectronic properties, and solar cell performance of both planar heterojunction and mesoporous Sb_2S_3 sensitized solar cells in the following sections.

2.2. Chemical methods

In chemical methods, the medium is prepared by using appropriate chemical compounds, including ionic solutions of the desired compound, solvents, surfactants, etc. Thermal/chemical treatments may be required after chemical compound deposition to achieve the desired phase. Chemical bath deposition (CBD) [64], spin coating [39], spray pyrolysis [33], electrodeposition [36], chemical vapor deposition (CVD) [65], dip-dry [66], and successive ionic layer adsorption and reaction method [67] have all been investigated to prepare Sb_2S_3 films (Table 2).

2.2.1. Chemical bath deposition

The chemical bath deposition (CBD) process is a solution-based synthesis method that has primarily been studied as a low-cost, convenient technique for large-area deposition of semiconductor thin film materials on various substrates.

In 1990, Sb_2S_3 was deposited by CBD for the first time using potassium antimony tartrate as an antimony source, thioacetamide as a reducing agent, and triethanolamine (TEA) as a complexing agent [101]. In this method, Sb_2S_3 was synthesized by reducing the $\text{Sb- triethanolamine}$ complex formed with thioacetamide. The resistivity of as-deposited Sb_2S_3 films was reported to be high and the thermal treatment of the Sb_2S_3 film in a nitrogen environment at 300 °C resulted in a decrease in resistivity due to sulfur loss during the annealing process, resulting in n -type behavior of the Sb_2S_3 film. Furthermore, heat treatment increases the grain size of Sb_2S_3 , improves crystallinity and decreases the bandgap [101]. Later, Savadogo et al. discovered that increasing the grain size of Sb_2S_3 through heat treatment reduces the grain boundary and hence the enhancement of the solar cell performance and the improvement was attributed to the decrease in grain boundary scattering, surface scattering, and space charge scattering as grain boundary area decreases [102]. Furthermore, the inclusion of Silicotungstic Acid (STA) in the Sb_2S_3 deposition process improved the photovoltaic properties due to the formation of energy states between the bandgap and facilitated charge transfer properties at the electrode interface [102]. Instead of using thioacetamide, by using $\text{Na}_2\text{S}_2\text{O}_3$ as a sulfur source, a uniform and compact thin film (0.3–0.4 μm) of Sb_2S_3 could be deposited in acidic (pH of around 2–3) or alkaline media (a pH of 8–10) in the presence of an EDTA complexing agent [103]. The deposition of Sb_2S_3 in acidic and alkaline media reveals a bandgap from 1.97 to 1.82 eV, respectively [103]. However, when

the Sb_2S_3 is formed in an aqueous medium, the formation of impurities has been reported due to hydrolysis reactions yielding SbOCl , $\text{Sb}(\text{OH})_3$, etc. [79,104] By changing the reaction medium to a non-aqueous 2-chloromethane, impurity-free Sb_2S_3 has been reported [105].

The use of various Sb and S sources, solvents, temperatures of the precursors and complexing agents has improved the quality of Sb_2S_3 films [79]. The formation of some Sb_2O_3 nanostructures on the surface of Sb_2S_3 in the air but not in N_2 indicates the importance of annealing conditions in obtaining Sb_2O_3 -free Sb_2S_3 films [106]. The effect of Sb concentration and annealing temperature on the quality of the Sb_2S_3 thin film was investigated by Srikanth [107] et al. and noted the increase in the grain size and the decrease in the

strain and dislocation density with the increase of antimony concentration. In their work, the particle size is found to be 2–4 μm with 0.1 M Sb, and by increasing the Sb concentrations further to 0.2 M, large-sized spherical grains of 8–10 μm in diameter have been reported, indicating particle growth at higher Sb concentrations and attributed to the growth mechanism involved in thin films. Further, it has been reported the decrease in bandgap with an increase in Sb concentrations is due to improved grain size growth and/or to a decrease in defect level. However, the mechanism of growth or how thickness affects crystalline size has not been clearly demonstrated [107]. On the other hand, it has been demonstrated that maintaining the pH at acidic levels of 2.3 and 2.53 results in better crystalline quality of Sb_2S_3 films [107].

Table 2
Performance of devices fabricated through different Sb_2S_3 fabrication methods.

| Deposition methods | Experimental conditions | Controlled property | Optimized condition of champion Sb_2S_3 cell | Photovoltaic parameters | | | | Ref | |
|---------------------------------------|--------------------------------------|--------------------------------------|--|-------------------------|---------------------------------|---------|--------|-------|------|
| | | | | PCE (%) | Jsc (mA/cm^2) | Voc (V) | FF (%) | | |
| ALD | Number of atomic cycle | Crystallinity | 150 cycles | 2.6 | 11.6 | 0.49 | 48.0 | [17] | |
| | Thickness of Sb_2S_3 | | 1600 cycles | 5.77 | 14.92 | 0.67 | 58.0 | [14] | |
| | Interfacial layer | | 54 nm | 3.4 | 13.5 | 0.62 | 41.0 | [68] | |
| CBD | Depositing time | Surface continuity | ZnS | 2.0 | — | — | — | [69] | |
| | Depositing time | Crystallinity | 3 h | 5.06 | 12.3 | 0.55 | 69.9 | [70] | |
| | Depositing time | Surface morphology and crystallinity | 4 h | 4.65 | 17.0 | 0.50 | 54.7 | [71] | |
| | Surface treatment | Surface morphology | DPA | 3.9 | 14.2 | 0.51 | 54.0 | [72] | |
| | Doping process | Coverage and crystallinity | Ti doped | 5.7 | 16.5 | 0.61 | 57.2 | [73] | |
| | Oxidation time | Surface morphology | 1 min | 2.4 | 9.1 | 0.62 | 41.9 | [74] | |
| | Doping process | Uniformity | Mn doped | 6.15 | 17.6 | 0.66 | 53.0 | [75] | |
| | Annealing process | Crystallinity | Annealed Sb_2S_3 | 1.78 | 4.83 | 0.66 | 55.8 | [76] | |
| | Surface treatment | Surface defect | TA + DPA | 3.23 | 10.31 | 0.55 | 57.0 | [77] | |
| | Spin coating | Surface treatment | Impurity phases | TA sulfurization | 7.5 | 16.1 | 0.71 | 65.0 | [11] |
| Spin coating cycles | | Crystallinity | 4 cycles | 2.3 | 8.12 | 0.62 | 45.9 | [78] | |
| SbCl_3 :TU ratio | | Grain size | 1:1.8 | 4.4 | 12.7 | 0.49 | 66.5 | [79] | |
| Annealing temperature | | Surface roughness and grain size | 300 °C | 4.3 | 12.9 | 0.63 | 52.4 | [54] | |
| SbCl_3 :TU ratio | | Grain growth and size | 1:1 | 2.65 | 9.43 | 0.56 | 50.3 | [39] | |
| SbCl_3 concentration | | Uniformity | 16 mg/ml | 6.27 | 14.73 | 0.65 | 65.7 | [80] | |
| Concentration of TU | | Surface coverage | 6 M | 5.69 | 14.34 | 0.66 | 60.4 | [81] | |
| Zn doping | | Crystallinity | 4.8% | 6.35 | 17.19 | 0.65 | 57.1 | [58] | |
| Alkali metal doping | | Crystallinity and grain size | Cs-doped | 6.56 | 17.3 | 0.69 | 55.2 | [82] | |
| Pre-annealing process | | Impurity phases | Under vacuum | 6.78 | 18.43 | 0.67 | 54.8 | [83] | |
| Doping process | | Surface uniformity | C_{60} doped | 1.75 | 8.44 | 0.49 | 42.2 | [84] | |
| Annealing temperature | | Crystallinity | 350 °C | 1.7 | 8.44 | 0.52 | 38.0 | [85] | |
| Spinning speeds | | Pin holes | 3000 rpm | 2.38 | 9.52 | 0.52 | 48.0 | [85] | |
| Interfacial layer (SbCl_3) | | Surface continuity | 30 mg/ml | 6.94 | 17.16 | 0.71 | 56.9 | [52] | |
| S/Sb ratio | | Surface morphology | 1.2 | 2.84 | 9.61 | 0.74 | 40.0 | [86] | |
| VTD | | Deposition temperature | Grain growth | 480 °C | 4.7 | 15.2 | 0.71 | 56.0 | [87] |
| | | Low temperature | — | 300 °C | 1.32 | 5.2 | 0.56 | 45.4 | [29] |
| Hydrothermal | Heating temperature | Grain size | 230 °C | 3.54 | 12.5 | 0.45 | 62.8 | [88] | |
| | Doping process | Crystal growth | Cd doped | 6.4 | 15.1 | 0.76 | 56.1 | [89] | |
| RF sputter | Annealing temperature | Crystallinity | 350 °C | 2.4 | 10.5 | 0.54 | 42.6 | [31] | |
| | Cu doping | Surface Uniformity | 8.6% | 1.13 | 5.17 | 0.49 | 44.6 | [90] | |
| | Surface treatment | Crystallinity and surface morphology | Selenization | 0.95 | 10.3 | 0.31 | 30.8 | [51] | |
| Spray pyrolysis | Thickness of Sb_2S_3 | Surface continuity | 100 nm | 3.7 | 10.3 | 0.69 | 52.0 | [91] | |
| | Annealing temperature | Crystallinity | 300 °C | 1.47 | 12.15 | 0.39 | 31.0 | [25] | |
| SIILAR | Interfacial layer | Homogeneity and rough surface | In_2S_3 | 4.9 | 7.8 | 0.55 | 58.0 | [92] | |
| | Thickness of Sb_2S_3 | Crystallinity | 62 nm | 5.69 | 14.3 | 0.66 | 60.4 | [81] | |
| Solvothermal | Amount of SbCl_3 | Grain size | 0.9 mmol | 3.46 | 12.5 | 0.45 | 61.7 | [93] | |
| | Thickness of Sb_2S_3 | Grain size | 450 nm | 1.27 | 6.1 | 0.6 | 35.0 | [94] | |
| Thermal evaporation | Depositing temperature | Grain size and growth | 550 °C | 2.37 | 8.21 | 0.68 | 45.3 | [95] | |
| | Thickness of Sb_2S_3 | Surface morphology | 100 nm | 1.69 | 6.5 | 0.59 | 44.0 | [50] | |
| | Crystallization temperature | Crystallinity | 300 °C | 2.48 | 11.1 | 0.52 | 43.1 | [28] | |
| | Surface treatment | Grain size and boundaries | Selenization | 3.22 | 10.2 | 0.57 | 55.3 | [28] | |
| | Pre-heating of substrate | Crystallinity | 320 °C | 3.01 | 10.9 | 0.59 | 46.8 | [96] | |
| | Thickness of Sb_2S_3 | Grain size | 800 nm | 2.86 | 10.9 | 0.58 | 45.3 | [97] | |
| | Surface treatment | Surface continuity | Selenization | 4.17 | 11.4 | 0.71 | 51.2 | [47] | |
| | Selenization time | Grain growth | 15 min | 2.13 | 8.8 | 0.52 | 46.4 | [98] | |
| | Substrate temperature | Grain growth | 300 °C | 1.29 | 5.9 | 0.58 | 37.8 | [99] | |
| | Doping process | Grain size and crystallinity | Sulfur doped | 5.8 | 16.2 | 0.71 | 50.7 | [100] | |

To investigate the Sb_2S_3 thickness dependence solar cell performance, Xiaoping et al. fabricated photoactive electrodes with thick and thin Sb_2S_3 -sensitized layers, polyaniline hole conductors, and counter electrodes [108]. Despite the presence of a large amount of Sb_2S_3 in thick film, the device with the thin Sb_2S_3 sensitized layer demonstrated an efficiency of 3.8%, while the thick Sb_2S_3 demonstrated an efficiency of 0.88%. The observed solar cell performance was primarily attributed to the deposition of a 3–5 nm thin layer of Sb_2S_3 on TiO_2 nanoparticles with diluted precursor concentrations, demonstrating the necessity of conformal deposition of Sb_2S_3 . As shown schematically in Fig. 4(a), the importance of having the well-aligned band between TiO_2 , Sb_2S_3 , and P3HT, as well as intimate contact between Sb_2S_3 and P3HT, for efficient transfer and collection of excited charge carriers was demonstrated by Chang et al. [70]. For further improvement of interface properties between Sb_2S_3 and P3HT, a porous P3HT layer was fabricated by adding 2,20-azobisisobutyronitrile (AIBN) as a nanopore-generating agent into the P3HT solution or blending Sb_2S_3 with P3HT and PCBM polymers [93]. The addition of a porous P3HT layer to an mp- $\text{TiO}_2/\text{Sb}_2\text{S}_3/\text{P3HT}$ heterojunction solar cell increased the efficiency by approximately 16% when compared to the flat or non-porous P3HT layer. The improvement was primarily attributed to an increase in charge collection efficiency due to the porous P3HT structure, which would extend the interface area between P3HT-Au and also P3HT- Sb_2S_3 , resulting in a reduction in charge transfer resistance between P3HT and the Au electrode as well as a shortening of the charge transfer time.

One of the major factors limiting the efficiency of m- $\text{TiO}_2/\text{Sb}_2\text{S}_3$ solar cells is the thickness of the light-harvesting layer, which cannot be increased to improve light harvesting because a thicker Sb_2S_3 results in a lower interfacial charge collection efficiency [110]. Hence, to address and optimize the thickness of the Sb_2S_3 layer, Cardoso et al. proposed the use of 1-D TiO_2 nanostructures (Fig. 4(b)) as such high surface area 1-D architectures provide a larger interface area, allowing the use of a thicker Sb_2S_3 film without sacrificing charge collection efficiency [71]. The crystal phase of the chemical bath deposited Sb_2S_3 thin films onto TiO_2 nanowires were found to be amorphous, producing Sb_2S_3 in the orthorhombic phase alone (310) plane oriented parallel to the substrate upon annealing in air, Ar or N_2 at temperatures above 250 °C. With an overall efficiency of 4.5%, the FTO/ TiO_2 nanowire $\text{Sb}_2\text{S}_3/\text{P3HT}/\text{PEDOT:PSS}/\text{Au}$ solar cells demonstrated a high short circuit photocurrent density (J_{sc}) of 17 mA cm^{-2} which has been attributed primarily to the rapid collection of photogenerated charges due to the 1-D nanowire geometry. However, the low V_{oc} of Sb_2S_3 solar cells based on 1-D TiO_2 nanostructures limited their efficiency, and further study has to be carried out to achieve a

higher V_{oc} [71]. However, it has been demonstrated a lower PCE for nanofibrous 1-D TiO_2 networks compared to 1-D TiO_2 nanotube [15]. In the latter case, a one-dimensional (1D) TiO_2 array is vertically oriented from the substrate allowing for vertical transport of photogenerated charges to the electrical contacts, whereas in the former case, nanofibrous 1-D TiO_2 is horizontally oriented from the substrate, preventing vertical charge transfer and thus better charge collection. It is known that the P3HT polymer co-absorbs light in the 450–650 nm wavelength range and the charge carriers generated by P3HT are not completely transferred to either the photoanode or the Au counter electrode [20,70]. The filtering effect of P3HT has been overcome by introducing PCBM as an additional electron channeling path in P3HT, allowing the transfer of charge carriers generated in P3HT to mp- TiO_2 , as shown in Fig. 4(c), where the addition of PCBM in P3HT improved the EQE in the 450–650 nm region [109]. Similarly, Chang et al. [109] demonstrated a 6.3% efficient solar cell by employing a low bandgap hole conducting PCPDTBT that can absorb light in the near-infrared region in a device structure of m- $\text{TiO}_2/\text{Sb}_2\text{S}_3/\text{PCPDTBT-PCBM}$. In contrast, Zimmermann et al. demonstrated chemical bath deposited flat junction Sb_2S_3 solar cells with an efficiency of 4% by addressing the issue of absorption losses in the hole transport material and outline a pathway toward more efficient future devices [18].

In an attempt to the tailoring of electronic band dispersion and improve carrier mobility, alloying of Sb_2S_3 with Bi has been demonstrated to be a successful approach as Sb and Bi have similar atomic orbitals and belong to group V [111,112]. Ito et al. introduced impurity materials into Sb_2S_3 to improve absorption and thus light-harvesting properties and noticed that Bi doping narrowed the Sb_2S_3 bandgap from 1.7 to 1.6 eV while Ti and Zn doping resulted in a slightly narrowed Sb_2S_3 band gap (Fig. 5(a)) [73]. However, as shown in Fig. 5(b) and (c), it has been noted the enhancement of photocurrent for Ti or Zn doped Sb_2S_3 thin films with CuCSN hole transport material, whereas Bi-doping resulted in photocurrent degradation due to aggregated Sb_2S_3 on the TiO_2 electrode [73]. Similarly, Mn-doped Sb_2S_3 was found to marginally improve the solar cell performance, which was attributed to improved spectral response due to the reduced band gap of Mn-doped Sb_2S_3 as well as reduced charge carrier recombination due to increased grain size of Mn-doped Sb_2S_3 [75].

The common issue in Sb_2S_3 thin films fabricated by the CBD method is the poor device performance due to the presence of surface defects in the Sb_2S_3 , such as sulfur vacancies caused by sulfur loss during the crystallization process, surface oxides (i.e. Sb_2O_3 and sulfates) caused by Sb_2S_3 oxidation and impurities such as SbOCl in Sb_2S_3 [13,113]. The presence of Sb_2O_3 or sulfur

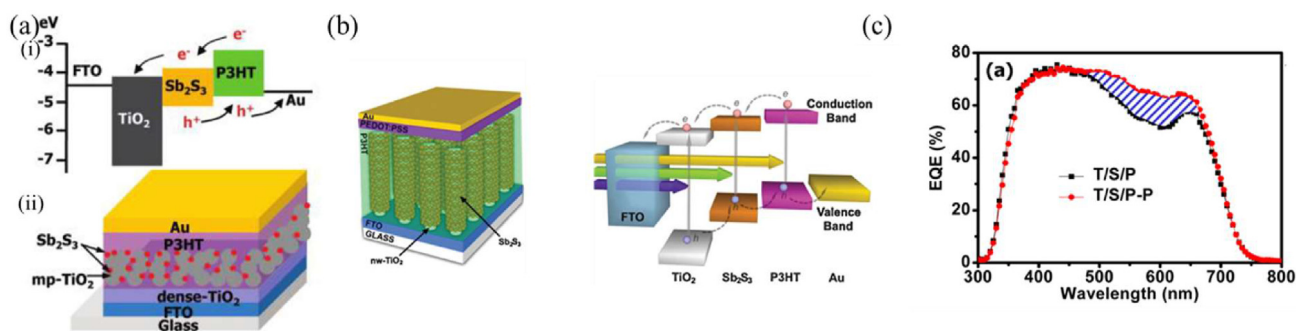


Fig. 4. (a) (i) Energy level diagram and (ii) Schematic diagram of FTO/dense- $\text{TiO}_2/\text{mp-TiO}_2/\text{Sb}_2\text{S}_3/\text{P3HT}/\text{Au}$ solar cell. Reproduced with permission. [70], 2010, American Chemical Society (b) Schematic diagram of the FTO/ TiO_2 nanowire array/ $\text{Sb}_2\text{S}_3/\text{P3HT}/\text{PEDOT:PSS}/\text{Au}$ thin-film solar cell and its energy level positions and charge transfer processes. Reproduced with permission [71], 2012, Royal Society of Chemistry (c) EQE spectra: the region marked by the blue lines is the EQE difference between the T/S/P-P and T/S/P samples: T = mp- TiO_2 , S = Sb_2S_3 , P = P3HT, and P-P = P3HT/PCBM. Reproduced with permission. [109], 2012, American Chemical Society.

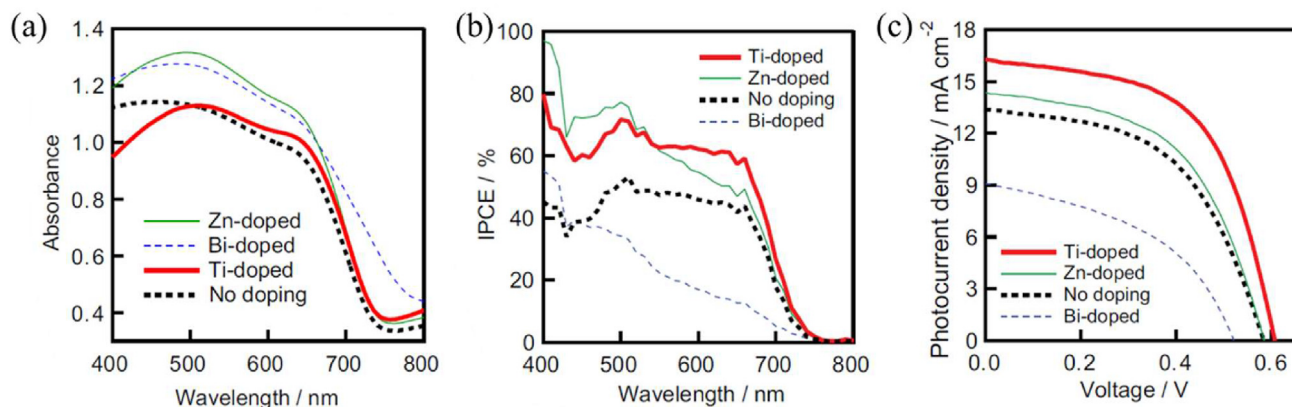


Fig. 5. (a) Absorption spectra of nanocrystalline-TiO₂/BaTiO₃/MgO/doped Sb₂S₃ layers. The amounts of dopants are 5 at% for Ti and Zn, and 3 at% for Bi. Reproduced with permission. [73], 2013, Elsevier. (b) IPCE spectra. Reproduced with permission. [73], 2013, Elsevier. (c) Current density–voltage (J–V) curves for (FTO glass/compact-TiO₂ nanocrystalline-TiO₂/BaTiO₃/MgO/doped Sb₂S₃/CuSCN/Au) solar cells. The amount of dopant is 5 at% for Ti and Zn, and 3 at% for Bi. Reproduced with permission [73], 2013, Elsevier.

deficiency could induce deep traps in Sb₂S₃, resulting in a lower power conversion efficiency as these defects act as the charge recombination centers. In particular, interface traps in Sb₂S₃ especially in the chemical bath deposited Sb₂S₃ which can reduce the external quantum efficiency by recombination of the separated carriers [6]. The trap sites were discovered to be located around an EC of -1.03 eV below the conduction band using the deep-level transient spectroscopy (DLTS) [114]. Kamat et al. demonstrated the presence of sulfide radicals in Sb₂S₃ that traps holes resulting in slow extraction of holes compared to electrons [13]. Hence, surface defects such as electron/hole trap sites should be reduced to improve the solar cell performance of Sb₂S₃-based solar cells. Intense efforts have been investigated to mitigate the charge recombination at the interface between TiO₂ and Sb₂S₃. i.e. Fukumoto [72] et al., treated the chemical bath deposited Sb₂S₃ with 1-decyl phosphonic acid (DPA) and noted a reduction in recombination as well as an increase in the open-circuit voltage and the fill factor. The reduction of charge recombination has been reported due to the blocking of recombination centers in both TiO₂ and Sb₂S₃ by attaching (masking, covering) the DPA to both the uncovered TiO₂ and the Sb₂S₃ surfaces [72]. On the other hand, Choi et al. [11] and Ye et al. [77] modified the chemical bath deposited Sb₂S₃ by Thioacetamide (TA)-based sulfurization to mitigate the sulfur vacancies and observed the suppression of the formation of Sb₂O₃ and the observed enhanced solar cell performance was

mainly attributed to the reduction of trap sites in Sb₂S₃. As shown in Fig. 6(a), before the TA treatment, diffraction peaks at 12.3° and 32° were due to the Sb₂O₃ phase and after TA treatment, they noted the transformation of Sb₂O₃ into a highly polycrystalline pure phase Sb₂S₃ structure. As shown in Fig. 6(b) Kang et al. introduced ZrO₂ and ZnS double blocking layers in between TiO₂/Sb₂S₃ (BL1) and Sb₂S₃/HTM (BL2), respectively and enhanced solar cell performance was reported [115]. The significant finding of this study was that Kang et al. were able to distinguish the TiO₂/Sb₂S₃ interface as the major charge recombination path rather than the Sb₂S₃/HTM interface. The function of BL1 was discovered to be blocking major charge recombination, which results in Voc enhancement, whereas BL2 causes the re-formation of Sb₂S₃ from surface oxidized Sb₂O₅ which affects the Jsc increment. A similar SiO₂ blocking layer was deposited on the TiO₂ to suppress charge recombination in the Sb₂S₃ solar cell, and Xu et al. reported the formation of irregular large Sb₂S₃ crystals on the porous and amorphous SiO₂ layer [116]. Although the formation of different sizes of Sb₂S₃ particles on SiO₂ may improve the light-harvesting properties, conformal coating of SiO₂ is required for efficient charge transport. Engelman et al. investigated the non-injected metal oxide-based Al₂O₃/Sb₂S₃ cells to suppress the charge recombination at the TiO₂/Sb₂S₃ interface [16]. In their study, electron injection into the oxide support was suppressed by using high-band gap Al₂O₃ as the supporting oxide, and thereby photogenerated charges were made to separate at the

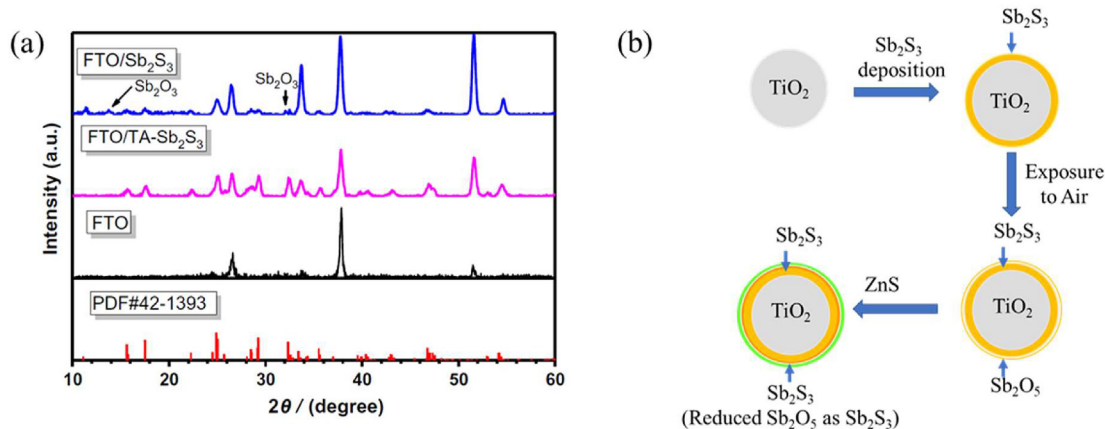


Fig. 6. (a) XRD patterns of FTO glass, FTO/Sb₂S₃ film and FTO/TA treated Sb₂S₃. Reproduced with permission [77], 2018, Elsevier. (b) Schematic diagram illustrates the surface reduction mechanism by ZnS. ZnS coating after air exposure convert the part of oxides as sulfides [115], 2014, Royal Society of Chemistry.

Sb₂S₃ layer reducing the recombination at the TiO₂/Sb₂S₃ surface and increasing the Voc to 0.71 V which is one of the highest reported values for Sb₂S₃ solar cell. However, the reported J_{sc} of the non-injected metal oxide-based Al₂O₃/Sb₂S₃ cell was lower than that of the TiO₂/Sb₂S₃ cell, which could be attributed to inefficient charge collection through the Sb₂S₃ layer.

On the other hand, to reduce trap density in Sb₂S₃, Godel et al. employed a modified CBD method in which the formation of Sb₂S₃ was slowed down by dissolving SbCl₃ in acetone and hydrolyzing with water under vigorous stirring to form Sb₄O₅Cl₂, Sb₈(OH)₆O₈Cl₂(H₂O), Sb₈O₁₁Cl₂(H₂O)₆ and Sb₃O₆(OH) and consequence addition of aqueous Na₂S₂O₃ to form amorphous Sb₂S₃ [104]. The reported crystalline properties of both modified CBD and CBD methods were found to be stibnite Sb₂S₃ having an average Sb₂S₃ crystallite size of 40 nm and 35 nm, respectively and achieved a 5.1% power conversion efficiency.

Despite the known negative effect of Sb₂O₃ formation during Sb₂S₃ synthesis [13,117], it has also been reported the improvement in solar cell performance due to the formation of Sb₂O₃ in Sb₂S₃ thin film annealed under N₂ at 300 °C for 30 min and cooled in the air [21,74,118]. The solar cell performance of the Sb₂S₃ film cooled under N₂ was 30% of the cell cooled under air. The improvement in solar cell performance was attributed to the formation of Sb₂O₃ in Sb₂S₃ in which the sample was immediately removed from the oven and cooled in air, resulting in the formation of Sb₂O₃ and the presence of some Sb₂O₃ was verified by the XRD analysis. The surface oxide presumably acts as a passivation layer, reducing electron–hole recombination. Further, they reported that the cell cooled under N₂ and then sintered at 200°C for 10 min in air showed the best performance [118]. Furthermore, a requirement of a buffer layer such as In–OH–S or a suitable high-band gap semiconductor in TiO₂-based ETA cells, particularly for relatively low-bandgap absorbers such as Sb₂S₃ has been demonstrated in the same study to stabilize the Sb₂S₃ properties. A similar charge recombination reduction between electrons in the Sb₂S₃ layer and holes in P3HT due to the formation of a Sb₂O₃ passivation layer by the partial oxidation of Sb₂S₃ during the annealing process, P3HT has been reported by Zhong et al. [15].

2.2.2. Spin coating

Though CBD is the most commonly used method for fabricating Sb₂S₃ thin film, it has inherent problems such as the formation of surface oxides (Sb₂O₃ and sulfates) and surface defects i.e. sulfur-deficits in Sb₂S₃ that cause the recombination of generated charge carriers, resulting in a lower power conversion efficiency [11]. Attempts have been made to improve the performance of hybrid solar cells by spin coating a defect-free Sb₂S₃ film [39,54,79]. You et al. reported the thermal decomposition of spin-coated Sb(thioacetamide: TA)₂Cl₃ on the bi-TiO₂/FTO substrate to produce oxide-free crystalline stibnite Sb₂S₃. A high molar ratio of Sb:S in the precursor Sb(TA)₂Cl₃ suppresses the formation of Sb₂O₃ due to the release of excess H₂S during the thermal decomposition of TA [78].

Despite the absence of Sb₂O₃ and sulfur vacancies in the spin-coated Sb₂S₃ films formed by the spin-coating method, the reported 2.1% device performance of FTO/bi-TiO₂/Sb₂S₃/P3HT/Au was lower than that of the CBD processed Sb₂S₃ film, demonstrating not only surface defects but also other factors are equally important for better device performance. However, Choi et al. on the other hand, reported a 6.4% efficient solar cell made by spin-coating an S/Sb ratio-controlled SbCl₃–thiourea complex solution into a mesoporous TiO₂ electrode to form defect-free Sb₂S₃ [79]. In their study, the formation of uniform and identical Sb₂S₃ structure along the depth of the m-TiO₂ layer was confirmed by the grazing incidence XRD (GIXRD) technique. The advantage of this method is that the S/

Sb ratio of the final product could be easily controlled and monitored to optimize the device performance, as shown in Fig. 7(a).

Gil et al. investigated the relationship between the morphology and photovoltaic properties of various Sb₂S₃ films fabricated by spin-coating precursor solutions containing SbCl₃ and thiourea onto the bi-TiO₂/FTO substrate by varying the concentration and the chemical composition of the precursor solutions as well as the spin coating cycle [39]. This study, demonstrated a closely related morphology variation of the Sb₂S₃ film to the precursor solution concentration and the compositional ratio of SbCl₃ and TU, and the morphology could be precisely controlled to obtain the desired Sb₂S₃ morphology. Aggregated free Sb₂S₃ were reported by spin coating with a low TU compositional ratio, whereas agglomerated Sb₂S₃ grains were observed at a high TU ratio due to rapid growth of Sb₂S₃ with a high TU ratio (Fig. 7(b)). Hence, the poor photovoltaic performance of Sb₂S₃ films fabricated with a higher TU composition ratio has been attributed to poor conductivity between the Sb₂S₃ grains. Later, Zhang et al. and Jin et al. detailed the material selection for the development of full inorganic solar cells based on Sb₂S₃, reporting 4.8 and 3.51% efficient solar cells for Sb₂S₃/V₂O₅ and Sb₂S₃/NiO planer heterojunction solar cells respectively [23,120]. Their study was focused primarily on V₂O₅ and NiO as an HTM and the structural properties of Sb₂S₃ crystals have not been fully described.

Instead of a single step, Zhang et al. employed sequential deposition in which the antimony acetate (Sb(Ac)₃) layer was spin-coated on the TiO–bi first, followed by thiourea solution and mild temperature annealing for the rapid deposition of high-quality Sb₂S₃ thin films without Sb₂O₃ formation [81]. The advantage of this method is no additional sulfurization of Sb₂S₃ film is required as the formation of Sb₂O₃ is greatly reduced due to the in-situ growth of Sb₂S₃ in a sulfur-rich environment, resulting in an optimized PCE of 5.69%. However, precise control of TU concentration is imperative as it would result in the formation of Sb₂S₃ films with sulfur vacancy leading to deep trap states at the low TU concentrations or Sb₂S₃ films with large pinholes in the Sb₂S₃ film at higher TU concentrations.

One of the most encountered problems in CBD-fabricated Sb₂S₃ films is a low fill factor caused by the formation of small Sb₂S₃ grains, resulting in a higher number of grain boundaries. To investigate the lateral grain size dependence photovoltaic properties, especially the fill factor, Wang et al. fabricated large Sb₂S₃ grain by a fast chemical approach in which the precursor Sb₂O₃ as Sb source in carbon disulfide (CS₂) and the n-butylamine mixed solution was spin-coated on the substrate [54]. By the variation of annealing temperature of the Sb₂S₃ films, the initially rough surface with many pinholes produced at low annealing temperature was switched to a smooth Sb₂S₃ surface with a very large lateral grain size up to 12 μm [54]. The reported 4.3% efficiency and 52.4% FF for fast growth Sb₂S₃ spin-coated films and 2.0% efficiency and 32.0% FF for CBD Sb₂S₃ films have been attributed to reduced grain boundaries, which result in improved fill factor of the solar cells and a higher PCE [54].

Although the large grain size is advantageous for charge transport across the film [54], it is not a desirable property for thin layered planar heterojunction solar cells due to the possibility of direct contact between the TiO₂ layer and back contact [53,85]. Similarly, rapidly grown Sb₂S₃ crystals were reported by Zheng et al. by spin-coating an antimony salt precursor in alcoholic solution onto an m-TiO₂ film and consequently transforming it to Sb₂S₃ by exposing it to H₂S and obtained homogeneously deposited pure Sb₂S₃ within the porous TiO₂ film [80]. The highest reported 6.2% power conversion efficiency in this study was found to be primarily related to the device's improved light-harvesting ability due to increased loading. On the other hand, Sung et al. optimized

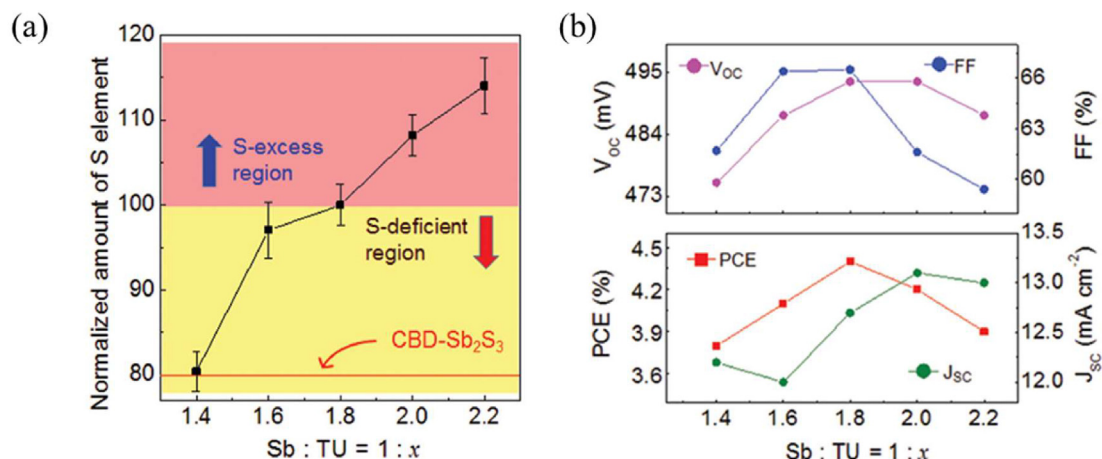


Fig. 7. (a) Normalized amount of S element in chemical bath deposited Sb₂S₃, Reproduced with permission [119], 2015, Wiley-VCH (b) values of V_{oc}, FF, J_{sc}, and PCE as a function of the SbCl₃:TU ratio. Reproduced with permission [119], Wiley-VCH.

the planar Sb₂S₃ solar cells through systematic engineering of the interface between TiO₂ and the Sb₂S₃ layer using a spin coating of the Sb₂S₃ layer [53]. In their study, the critical role of the interface between m-TiO₂ and Sb₂S₃ in the device performance was demonstrated by fabricating planar Sb₂S₃ solar cells with different interfacial structures by manipulating the nanostructures of the TiO₂ photoelectrode and the Sb₂S₃ absorber layer. In their investigation, they demonstrated why the device performance of spin-coated Sb₂S₃ film is superior to CBD Sb₂S₃ in planar Sb₂S₃ solar cells, as well as why rough TiO₂-bl is preferred over flat TiO₂-bl in spin-coated Sb₂S₃. The CBD-formed Sb₂S₃ thin film, as shown in Fig. 8(a), is composed of agglomerated Sb₂S₃ grains, whereas the spin-coated Sb₂S₃ film is composed of smooth and dense Sb₂S₃ grains. Importantly, Sung et al. [53] demonstrated the importance of intimate contact between the TiO₂ photoelectrode and the Sb₂S₃ absorber layer, as well as continuous connectivity of the absorber layer, for Sb₂S₃ planar cell device performance.

Contrary to the known negative effect of sulfur vacancies in Sb₂S₃, which acts as charge recombination centers, Tang et al. reported the enhancement of solar cell performance by introducing ZnCl₂ in the precursor materials to generate sulfur vacancies leading to an increase in the electron concentration and consequent decrease in the series resistance in Sb₂S₃ [58]. Also, the enhanced PCE was attributed to the elevated Fermi energy level as a result of the increased carrier concentrations in Zn doped Sb₂S₃, which would facilitate the charge transport from Sb₂S₃ to TiO₂ compared

to that of pristine Sb₂S₃ (Fig. 8(b)). Hence, the sulfur vacancies in Sb₂S₃ could have dual functions; as a carrier recombination center, lowering solar cell performance, and as an increase in electron concentration, increasing solar cell performance, opening up new avenues for optimizing device performance by carefully manipulating the intrinsic defects in Sb₂S₃. Although the enhanced solar cell performance of Zn-doped Sb₂S₃ was solely attributed to the increase in electron concentration, the reduction of recombination sites in Sb₂S₃ i. e. V_{sb} defects sites by Zn doping also has to be considered.

To address the poor quality and high trap states of Sb₂S₃ films, which limit the device performance of Sb₂S₃ films formed by spin coating, additives have been introduced to the Sb-precursor source, which could coordinate with Sb atoms via multidentate anchoring and annihilate the trap states. By adding additive 4-Chloro-3-nitrobenzenesulfonyl chloride (CSCI), which contains two terminal Cl with lone pair of electrons that can interact with Sb atoms, low-resistivity Sb₂S₃ film with enhanced crystallization (Fig. 9(a) and (b)) and low trap states was reported by Zhou et al. [121] The CSCI additive raises the Fermi level of the Sb₂S₃ film, which improves electron transport from Sb₂S₃ to TiO₂ (Fig. 9(c)). As a result, the optimal PCE of Sb₂S₃ solar cells is increased from 4.20 to 5.84%. Similarly, Han et al. demonstrated that using a multidentate ionic liquid, tetramethylammonium hexafluorophosphate ([TMA][PF₆]), which contains six different oriented fluorine atoms with lone pair of electrons, can reduce the crystallization rate and significantly

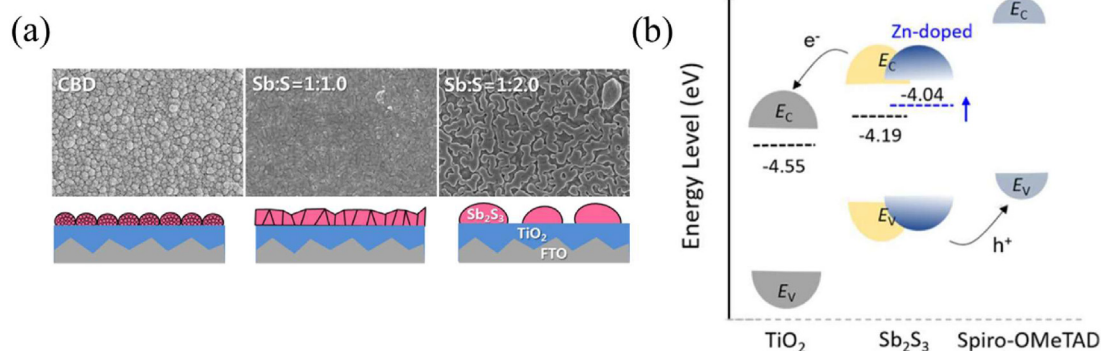


Fig. 8. (a) SEM images and schematic diagrams of CBD and spin-coated Sb₂S₃ absorbers on a flat TiO₂ blocking layer. Reproduced with permission [53], 2017, Science Direct. (b) Energy level diagram of the device with Sb₂S₃ and Zn-doped Sb₂S₃ as light absorption materials. Reproduced with permission [58], 2018, American Chemical Society.

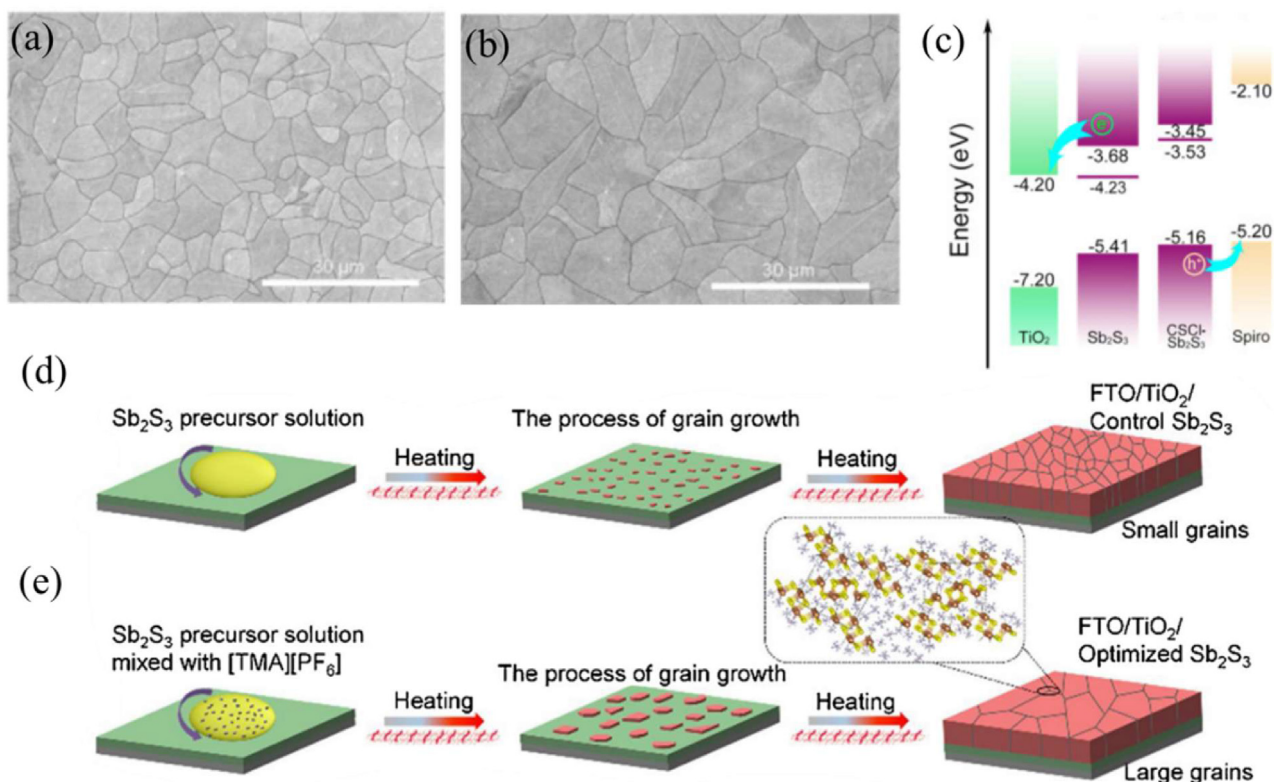


Fig. 9. Top-view surface micrographs of (a) the control Sb_2S_3 and (b) $\text{CSCI-Sb}_2\text{S}_3$ films. Reproduced with permission [121], 2021, Elsevier. (c) Energy band diagram of $\text{TiO}_2/\text{Sb}_2\text{S}_3/\text{Spiro-OMeTAD}$. Reproduced with permission [121], 2021, Elsevier. (d) The schematic about the crystallization process of the control Sb_2S_3 and (e) The schematic about the crystallization process of optimized Sb_2S_3 . Yellow, brown, purple and gray spheres represent S, Sb, P and F, respectively. Reproduced with permission [122], 2021, Elsevier.

increase the grain size of Sb_2S_3 by coordinating with Sb atoms due to increasing in the critical Gibbs free energy of nucleation as shown in Fig. 9(d) and (e) [122]. As a result of improved crystalline quality and trap states, Han et al. achieved a PCE of 6.63% with an optimum of 10% [TMA] [PF₆], due to improved crystalline quality and low-trap states, lowering resistivity and raising the Fermi level of the Sb_2S_3 , allowing for effective charge transfer.

Similarly, doping K, Rb and Cs in Sb_2S_3 was also found to improve solar cell performance, owing to an increase in charge concentration, crystalline size, crystallinity, and high-film quality (Fig. 10(a)), whereas Li and Na doping degrades device performance due to pinholes and cracks in the Sb_2S_3 film [82]. Similar to Zn doping in Sb_2S_3 , alkali metals form a chemical bond between alkali metals and sulfur at the grain boundaries of Sb_2S_3 , raising the Fermi energy level and resulting in a PCE of 6.56% for Cs-doped Sb_2S_3 [82].

It is well known that 1-D nanostructures can improve charge collection efficiency. As a result, variations in the charge collection efficiency of Sb_2S_3 on different 1-D nanostructures have been observed by spin coating $\text{SbCl}_3:\text{TU}$ solutions on different 1-D TiO_2 nanostructures [83,124]. As shown in Fig. 10(b), Tan et al. demonstrated that using a vacuum-assisted solution processing approach leading to the formation of homogeneous and aggregated less Sb_2S_3 performance from 4.15 to 6.78%. The formation of highly crystalline, high surface coverage and phase purity Sb_2S_3 film has been reported by careful modification of pre-annealing of Sb_2S_3 films formed by spin coating of Sb-TU complex on top of a 1-D TiO_2 nanorod array [83]. The removal of organic solvent by the pre-heating process was found to be the reason to yield better optoelectronic properties of the devices. As a result, the photocurrent, as well as fill factor of the device, are enhanced resulting in the enhancement of overall solar cell performance [83]. By similar pre-

annealing conditions, later, Kaienburg et al. reported the reduction of pinholes in Sb_2S_3 films formed by spin coating of Sb-TU precursor solution using similar pre-annealing conditions. In addition, instead of Sb-TU, they used an antimony-butyldithiocarbamate (Sb-BDC) complex precursor to create a pinhole-free Sb_2S_3 layer with large grain size (Fig. 10(c)) [123].

In another study, Chen et al. investigated in situ-grown monolayer of large [221]-oriented Sb_2S_3 cuboids on a polycrystalline TiO_2 nanoparticle film to enhance the charge transport channels inside the Sb_2S_3 layer [125]. The critical factors for the preferentially-oriented growth of Sb_2S_3 cuboids have been detailed in their study in which both the TiO_2 surface and Sb precursor control the growth and the orientation of Sb_2S_3 crystals. It has been noted the growth of irregular and larger Sb_2S_3 grains with no preferential orientation in the absence of Sb_2S_3 crystalline seeds while with Sb_2S_3 crystalline seeds on the TiO_2 film surface the Sb_2S_3 cuboids are growths along the [001], [010], and [100] directions with the (001) and (100)/(010) planes tilting the average angles of ca. 44° and 61° on the substrate, respectively as shown schematically in Fig. 11(a) and SEM image in Fig. 11(b). The reported solar cell efficiencies of $\text{Sb}_2\text{S}_3/\text{TiO}_2$ -bulk/nanoplanar heterojunction (BnPHJ) solar cells for oriented and non-oriented growth Sb_2S_3 films were 5.15% and 3.62%, respectively and were mainly attributed to the observed shorter electron collection time for the oriented growth Sb_2S_3 film. Tamilselvan et al. demonstrated the importance of forming ribbon-like horizontally stacked Sb_2S_3 with planes either with $hkl: l = 0$ or $l \neq 0$ for optimum light harvesting as well as charge collection [85]. The higher PCE observed for Sb_2S_3 films fabricated using a metal-organic precursor (metal-butyldithiocarbamate) at higher temperature was attributed to the formation of $hkl: l \neq 0$ Sb_2S_3 structures which was evidenced

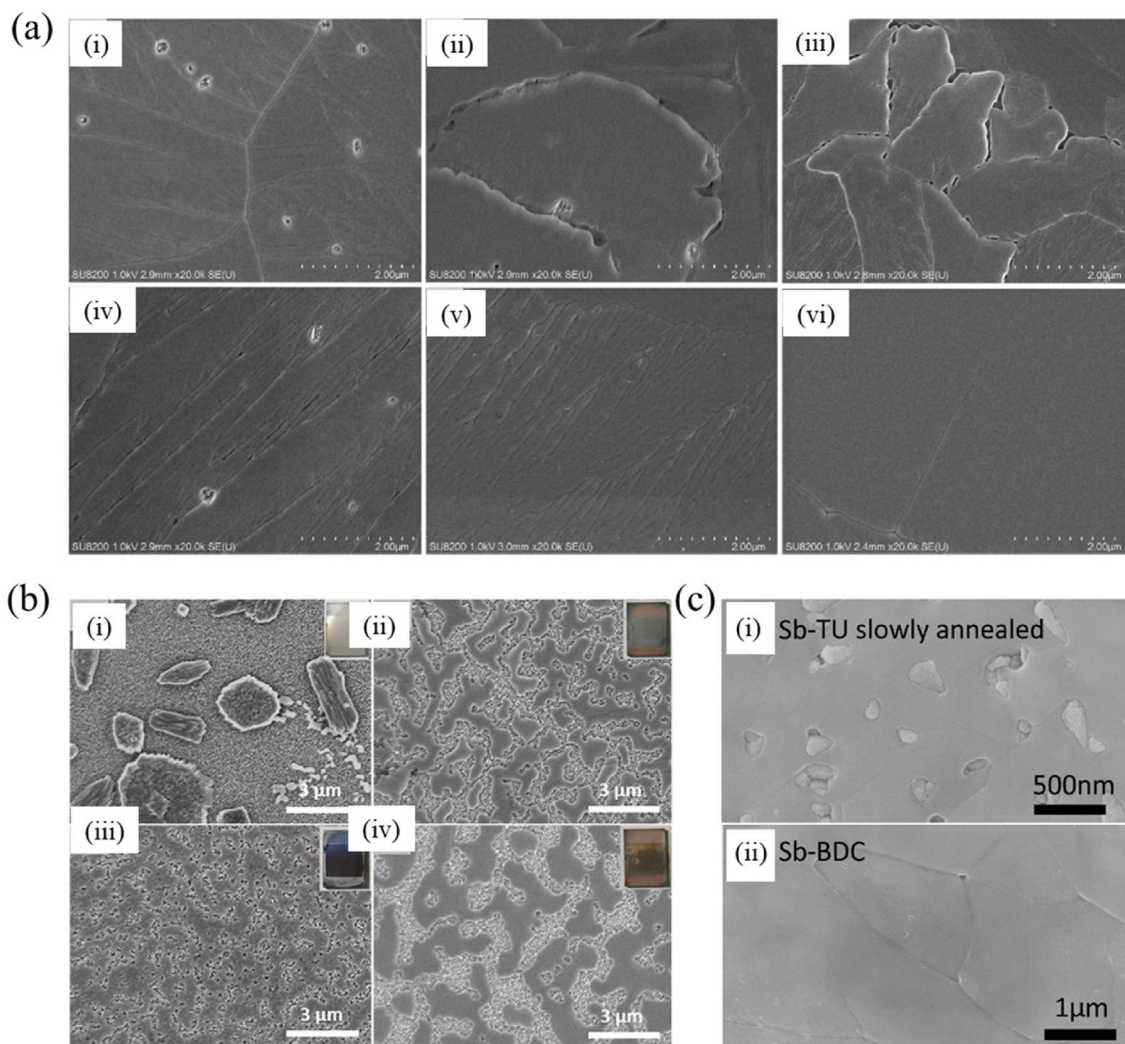


Fig. 10. (a) SEM images of (i) pristine Sb_2S_3 , (ii) Li-doped Sb_2S_3 film, (iii) Na-doped Sb_2S_3 film, (iv) K-doped Sb_2S_3 film, (v) Rb-doped Sb_2S_3 film, and (vi) Cs-doped Sb_2S_3 film. Reproduced with permission [82], 2018, Wiley-VCH. (b) SEM images of the surface morphologies of (i, ii) conventional process (CP)– Sb_2S_3 with pre-annealing at 125 and 150 °C, (iii, iv) vacuum-assisted solution process (VASP)– Sb_2S_3 films with pre-annealing at 125 and 150 °C [83], 2018, Royal Society of Chemistry. (c) SEM images of Sb_2S_3 thin films after crystallization at 265 °C: (i) An intermediate slow annealing step at 100 °C for 60 min reduces the pinhole area, (ii) The Sb-BDC based process leads to a compact layer with large grains and without pinholes. Reproduced under terms of the CC-BY license, [123].

by the Sb_2S_3 XRD pattern (Fig. 11(c)) where it was observed higher intensity for (hk0) planes (020), (120), (130) in comparison to (hkl) planes (211), (221). The same authors later developed a PTB7/ Sb_2S_3 /TiO₂-nanoarray p-i-n heterojunction (NHJ) device to improve light absorption and charge transport properties, employing a seed-assisted repetition of spin-coating and annealing (RSCA) strategy to produce preferentially Sb_2S_3 single-crystalline nanorods [211]-oriented and vertically aligned on polycrystalline TiO₂ nanoparticle film. Covalently bound (Sb_4S_6)n ribbons in [211]-oriented single-crystalline Sb_2S_3 nanorods in the p-i-nNHJ device provide effective charge transport channels for the photogenerated charge carriers inside the Sb_2S_3 layer to efficiently reach the collection electrode and no negative Eph effects resulting in a long electron lifetime on the sub-second scale ($\tau_{e1} \approx 0.9$ s) due to the absence of photogenerated hole accumulation on around Sb_2S_3 nanorods, making the PTB7/ Sb_2S_3 /TiO₂ NHJ have a good application potential to efficient solar cells [126].

The dependence and control of the quality of Sb_2S_3 films have been reported by optimization of different Sb_2S_3 preparation conditions as well as comparison of different precursor solutions such as SbCl_3 and TU or antimony oxide (Sb_2O_3) and butyldithiocarbamic

acid BDCA [123]. Phase purity crystalline Sb_2S_3 film with high surface coverage has been reported by changing several key experimental factors (i.e. precursor concentration, an optimized ratio of the component in precursor solution, crystallization temperature, annealing procedure, annealing environment, the thickness of a hole-blocking layer, etc) during Sb_2S_3 deposition. On the other hand, enhanced PCE was reported for C60 incorporated Sb_2S_3 thin films and the enhanced efficiency was mainly attributed to the enhanced conductivity of C60– Sb_2S_3 thin films than that of pure Sb_2S_3 films [84].

Several research groups reported improved PCE of Sb_2S_3 -based solar cells by reducing defects in Sb_2S_3 fabricated by the spin coating followed by post-treatment of Sb_2S_3 films. Han et al. reported the post-treatment of Sb_2S_3 films with an inorganic SbCl_3 salt, which passivates the Sb_2S_3 via the interactions of Sb and Cl in SbCl_3 molecules with S and Sb in Sb_2S_3 , respectively resulting in suppression of nonradiative recombination in Sb_2S_3 film [52]. The reported valence band maximum of SbCl_3 and Sb_2S_3 were –5.22 and –6.85 eV respectively, allowing photogenerated holes to be transferred into Spiro-OMeTAD through the thin SbCl_3 layer while preventing charge recombination and thus improving charge

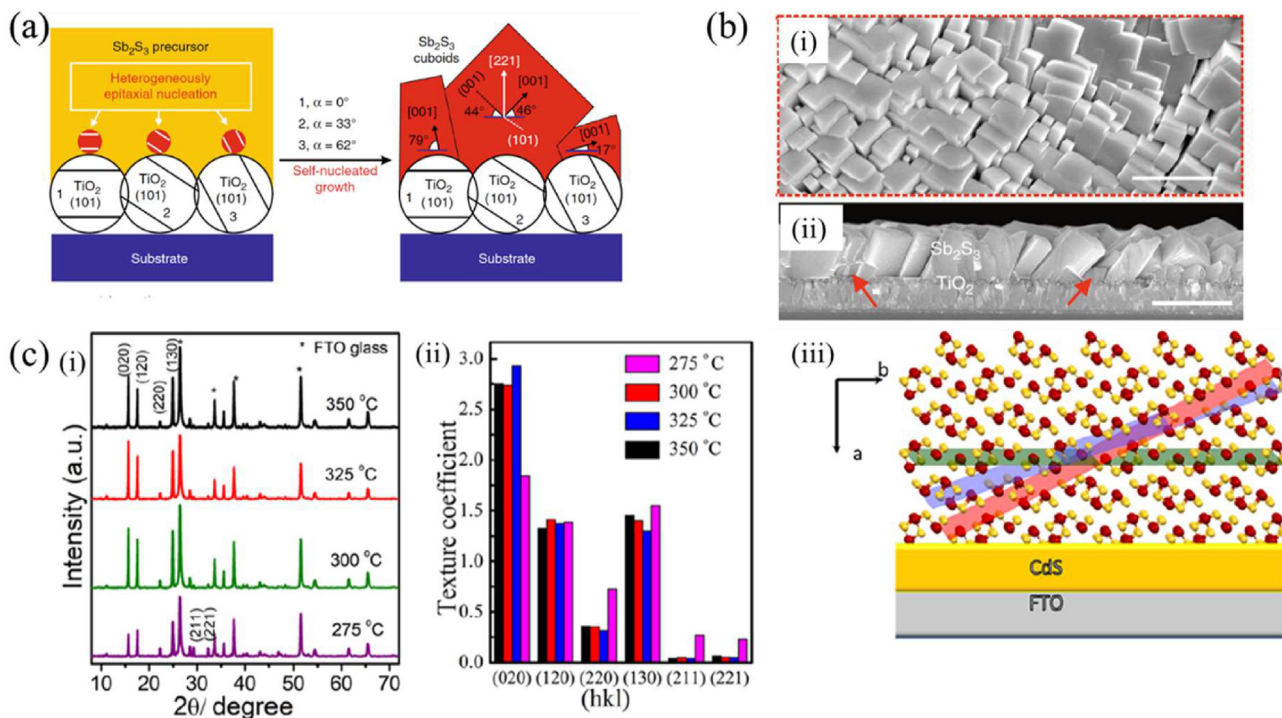


Fig. 11. (a) Schematic illustration of the OCE nucleation/growth model for the growth of Sb_2S_3 single-crystalline cuboids on polycrystalline TiO_2 nanoparticle film, where the most competitive TiO_2 nanoparticle orientation for the Sb_2S_3 single-crystals to nucleate/grow features its (101) plane tilting an angle (α) on substrate plane close to $\alpha = 33^\circ$ (Particle 2), but the nucleation/growth at other sites around (e.g., particle 1 of $\alpha = 0^\circ$ and Particle 3 of $\alpha = 62^\circ$) is relatively much slower or suppressed due to their unfavorable TiO_2 (101) plane orientations. Reproduced under terms of the CC-BY license [125], (b) (i) magnified Bird-view image of Sb_2S_3/TiO_2 -bulk/nano planar heterojunction and (ii) cross-sectional SEM images of as-prepared Sb_2S_3/TiO_2 -bulk/nano planar heterojunction on FTO substrate. Reproduced under terms of the CC-BY license [125], (c) (i) Temperature-dependent powder XRD patterns of as-prepared Sb_2S_3 . (ii) Texture coefficient (TC) of selected diffraction peaks in Sb_2S_3 thin film at different temperatures. (iii) Schematic presentation of horizontal packing of $[Sb_4S_6]_n$ ribbon structure on the CdS/FTO substrate while viewing along the c-axis. Rectangle strips represent the planes [green: (020), red: (120), blue: (130)]. Reproduced with permission [85], 2019, American Chemical Society.

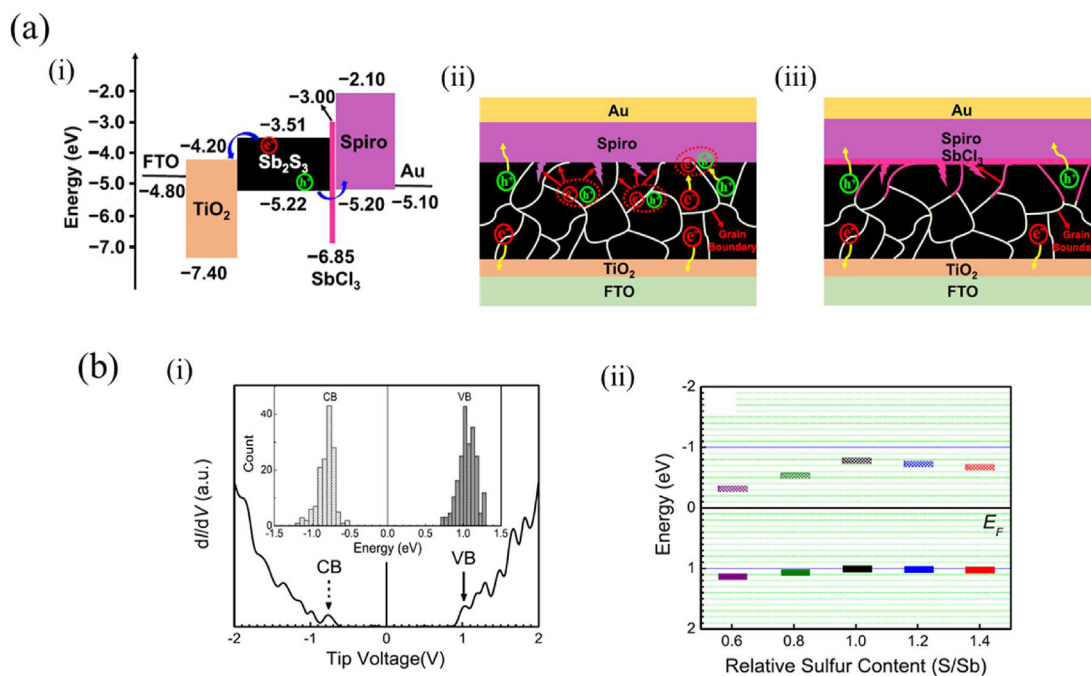


Fig. 12. (a) (i) Energy band diagram of the various layers in the passivation device and the charge transfer at the interface of $Sb_2S_3/Spiro$ -OMeTAD, (ii) Schematic diagram of charge transfer in the control device and (iii) the $SbCl_3$ -treated Sb_2S_3 device. Reproduced with permission [52], 2020, American Chemical Society (b) (i) dI/dV spectrum of pristine Sb_2S_3 thin films and (ii) band edges of vacancy-tailored Sb_2S_3 thin films. The inset of panel a shows the histogram of the band edges. Reproduced with permission [86], 2020, American Chemical Society.

collection efficiency as shown in Fig. 12(a)(i, ii, iii). Furthermore, the observed 7.1% efficiency which was the highest for Sb_2S_3 -based solar cells primarily attributed to sulfur-vacancy (trap state) passivation at grain boundaries or interfaces of Sb_2S_3 [52]. The function of the surface modifier was found to be preventing direct contact between TiO_2 and spiro-OMeTAD by further absorbing the surface modifier on the bare TiO_2 surface that was not covered by the Sb_2S_3 particles. On the other hand, a modified two-step sequential deposition method was reported by Maiti et al., For the passivation of sulfur vacancies by maintaining a slightly higher sulfur-rich condition S/Sb ratio during Sb_2S_3 film formation [86]. By scanning tunneling spectroscopy (STS) measurements, a blue shift of conduction band (CB)-edge away from the Fermi energy and widen of the transport gap of Sb_2S_3 was reported until the relative sulfur content in the semiconductor reached a stoichiometrically-balanced condition (S/Sb = 1.0) and with a further increase in sulfur-content (S/Sb = 1.2 and 1.4), the band gap of Sb_2S_3 was found to decrease (Fig. 12(b)(i and ii)) while surface roughness increase with the increase of S/Sb ratio. The observed highest 3.1% PCE observed at a S/Sb ratio of 1:2 was mainly a result of an optimization of the optical bandgap and surface morphology.

2.2.3. Other chemical methods

As previously stated, the vast majority of Sb_2S_3 thin films have been produced using common chemical deposition methods such as CBD and spin coating methods, with only a few reports on spray pyrolysis, SILAR, solvothermal, hydrothermal, electrodeposition, sol-gel, and dip coating methods. These methods will be discussed briefly in the sections that follow.

2.2.3.1. Spray pyrolysis. The chemical spray pyrolysis (CSP) process is a more adaptable process that allows for easy modification of material properties such as stoichiometric ratio, phase composition, particle size, specific surface area, etc. In 1991, Bhosale et al. reported the deposition of Sb_2S_3 thin films on FTO glass by spray pyrolyzing antimony trichloride and thioacetamide with oxalic acid or acetic acid as the complexing agent [127]. The formation of polycrystalline and n-type amorphous Sb_2S_3 with both oxalic and acetic acids has been reported, while the bandgap increased from 1.5 to 1.8 eV when the complexing agent was changed from oxalic to acetic acid. Rajpure et al. investigated the effects of the precursor and complexing agent concentration on Sb_2S_3 properties [128]. It was demonstrated that the optimization of crystalline properties of Sb_2S_3 by using different Sb:S volume ratios in the solution 1:9, 2:8, 3:7, 4:6, 5:5, 6:4, 7:3, 8:2, and 9:1, in which the highest crystallinity and grain size were noted for 4:6 Sb:S ratio due to agglomeration of particles. The same research group reported that changing the precursor solvent from aqueous to non-aqueous solvents changed the conductivity from n- Sb_2S_3 to p- Sb_2S_3 as well as amorphous to polycrystalline, indicating that the solvent properties can be used to effectively control and obtain the desired Sb_2S_3 properties for the desired application [128].

The single-phase stoichiometric Sb_2S_3 is an essential requirement for the application of Sb_2S_3 in solar cells and the growth of single-phase stoichiometric Sb_2S_3 crystals, Kärber et al. employed ultrasonic chemical spray pyrolysis (ultrasonic CSP) process [33]. The advantage of the ultrasonic CSP process to produce sub-micrometer size single-phase crystalline Sb_2S_3 particulates without antimony hydroxide formation and post-deposition heat treatment was demonstrated by Karber et al. Despite the fact that the ultrasonic CSP process yielded defect-free Sb_2S_3 nanoparticles, the reported 1.9% conversion efficiency for glass-ITO- TiO_2 - Sb_2S_3 -P3HT-Au is not comparable to other reported similar device structures, which may arouse as a result of incomplete coverage of TiO_2 surface by light-harvesting Sb_2S_3 due to the rapid growth of

Sb_2S_3 crystal [129]. To form a continuous and uniform transparent Sb_2S_3 layer on TiO_2 (Fig. 13(a)), later they employed a two-step sequence, whereby amorphous Sb_2S_3 layers were first deposited by USP and then crystallized by thermal annealing [91,129]. A reported PCE of 5.5% at AM1.5G for a 1.7 mm² semitransparent ITO/ TiO_2 / Sb_2S_3 /P3HT/Au cell, and only 3.2% decrease in the scale-up from mm² to cm² while retaining the 70% efficiency after one year of non-encapsulated storage ensure their potential for application in semitransparent solar windows.

Hector et al. used an ITO/ZnO/ TiO_2 / Sb_2S_3 /P3HT/Au core-shell NW heterostructure device structure with ZnO (NW)/ TiO_2 (passivation layer) and a thin-film of Sb_2S_3 grown by the CSP process to mitigate the charge carrier losses and passivation. The Sb_2S_3 film grown on the ZnO(NW)/ TiO_2 (passivation layer) is highly pure and free of unwanted Sb_2O_3 phases, and crystallinity is reported to be highly dependent on Sb_2S_3 film thickness, with amorphous Sb_2S_3 films formed at a few nanometers and crystalline films formed at several tens of nanometers. However, the highest reported efficiency with the intermediate optimum thickness of the Sb_2S_3 shell was 2.83%, which was limited by the balance of crystallinity and defect density [130]. According to Fig. 13(b), a Volmer-Weber growth mechanism path has been proposed for the growth of transparent Sb_2S_3 film during ultrasonic CSP. At an optimized deposition temperature, the molar ratio of precursors SbCl_3 and thiourea, and the post-deposition treatment temperature, a uniform pinhole-free polycrystalline orthorhombic Sb_2S_3 thin-film with lateral grain size ~10 μm have been reported by crystallization of amorphous Sb_2S_3 layers in vacuum at 170 °C for 5 min.

2.2.3.2. SILAR. The SILAR (Sequential ionic layer adsorption and reaction) method is similar to the CBD process in that the substrate is immersed in separate cation and anion precursor solutions, with each immersion followed by rinsing with a suitable solvent [131]. It has been used successfully to deposit q-dots of sulfide compounds and is also regarded as one of the most effective methods of precisely controlling the deposition of QDs.

The application of the SILAR technique to fabricate Sb_2S_3 -based solar cells was successfully demonstrated by Huerta-Flores et al., in which an ~80 nm extremely thin layer of In_2S_3 - Sb_2S_3 was deposited on the mesoporous TiO_2 by SILAR and a PCE of 4.9% was reported for the device structure ITO/ TiO_2 / In_2S_3 - Sb_2S_3 /CuSCN/Au [92]. To precise control of M_2S_3 deposition, Yoo et al. employed a two-step template method in which either CdS or ZnS layer was first deposited onto TiO_2 layer and by dipping CdS-coated TiO_2 film into an M source solution for several minutes to convert CdS or ZnS into M_2S_3 by a cation-exchange process [132]. As shown in Fig. 14(a), the reported rapid color change from yellow color to the different one of the targets QDs was attributed to the exchange of Cd with the target QDs. By HRTEM analysis, the authors demonstrated the formation of discrete Sb_2S_3 nanoparticles on the TiO_2 surface and a 3.69% PCE has been reported for an optimized Sb_2S_3 -sensitized solar cell fabricated by the cation exchange method. However, the reported low PCE performance could be due to the non-conformal coating of Sb_2S_3 on TiO_2 resulting in lower loading of the light-harvesting Sb_2S_3 , and to improve the PCE of template deposited Sb_2S_3 , the Sb_2S_3 loading amount has to be enhanced.

To address the Sb_2S_3 loading amount and enhance the charge carrier transport, Zhang et al. fabricated a hybrid inorganic-organic heterojunction solar cells using Sb_2S_3 as a light-absorbing semiconductor, TiO_2 nanorods(NRs), P3HT as both a hole conductor and light absorber [133]. The reported PCEs of short and long TiO_2 NRs were 1.84 and 0.28% respectively and the dependence of PCE on the length of TiO_2 NRs has been mainly attributed to hindered charge carrier transport due to the coaxial structure of Sb_2S_3 on the TiO_2 NR (Fig. 14(b)). However, as previously stated, the reported low

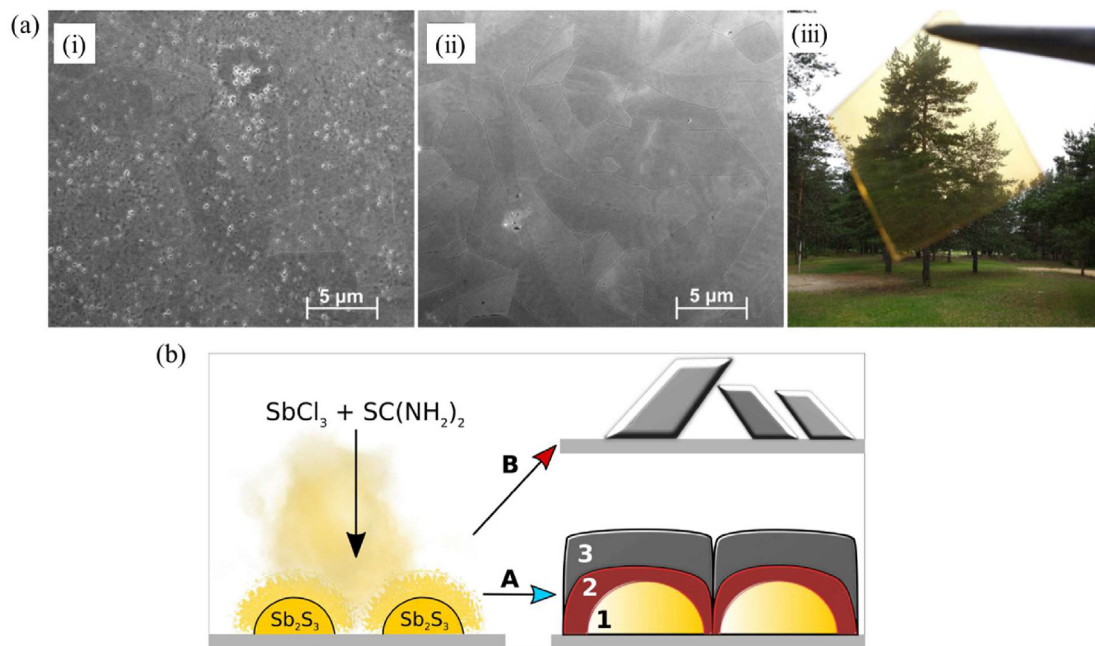


Fig. 13. (a) Surface views, by scanning electron microscopy (SEM) of (i) 70 nm and (ii) 100 nm thick annealed Sb_2S_3 layers on a glass/ITO/ TiO_2 substrate. (iii) Photograph of a 5×5 cm semitransparent (AVT 26%) stack of glass/ITO/ TiO_2 /100 nm annealed Sb_2S_3 . Reproduced under terms of the CC-BY license [91], (b) Proposed growth mechanism paths of Sb_2S_3 by Volmer–Weber growth during ultrasonic spraying of methanolic solution of $SbCl_3$ – $SC(NH_2)_2$ in excess of sulfur precursor in an aerosol. Reproduced under terms of the CC-BY license, [129].

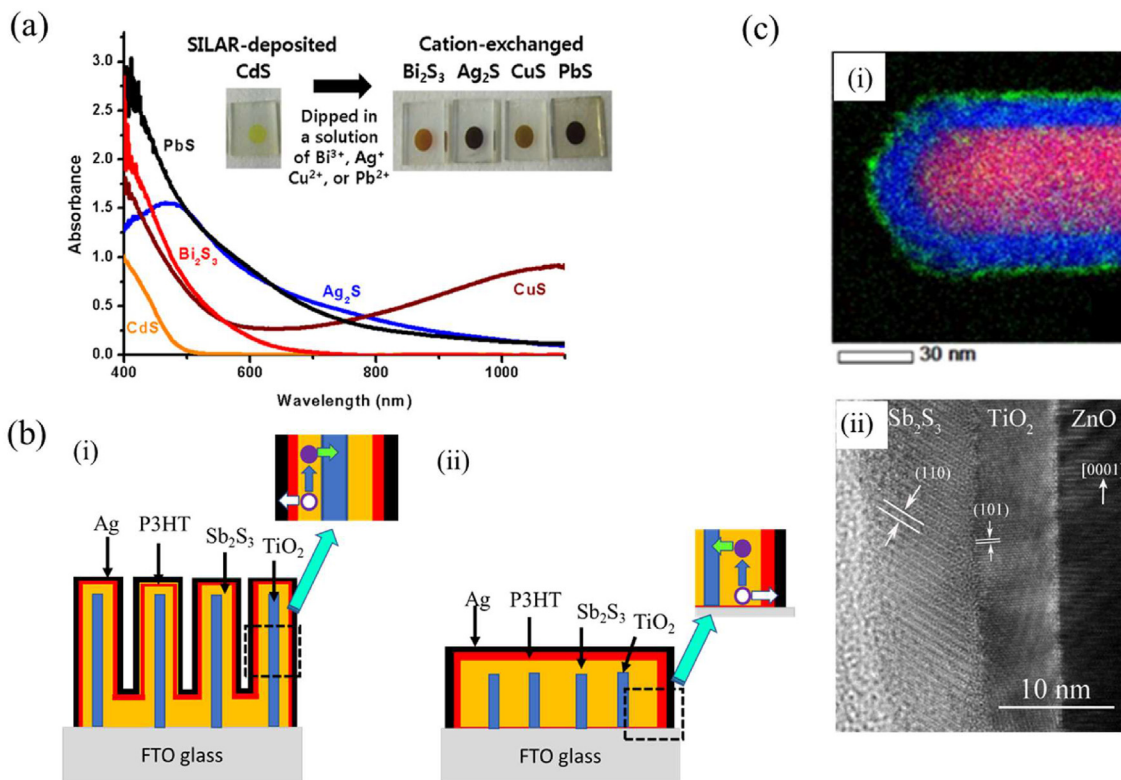


Fig. 14. (a) Absorption spectra of SILAR-deposited CdS QD and its converted ones (Bi_2S_3 , Ag_2S , CuS , and PbS) by a cation exchange process over mesoporous TiO_2 film/FTO electrode and a picture of as-obtained electrodes (inset) [132]. (b) Schematic device structure with (i) long TiO_2 NRs and (ii) short TiO_2 NRs of the improved photovoltaic performance [133], 2017, Springer (c)(i) EDS-STEM elemental mapping superimposing the zinc, titanium, and antimony element signals. (ii) HRTEM image of $ZnO/TiO_2/Sb_2S_3$ core shell NW heterostructures annealed at $300^\circ C$ for 5 min under flowing nitrogen atmosphere with a special focus on a small cluster in the Sb_2S_3 absorbing shell. Reproduced with permission [134], 2017, American chemical society.

efficiencies for Sb_2S_3 solar cells fabricated using the SILAR process and 1-D TiO_2 as an electron transport medium could be primarily due to the incomplete coating. Though the SILAR process is expected to form a conformal coating of Sb_2S_3 on TiO_2 NR, the formation of Sb_2S_3 clusters or agglomerates on top of TiO_2 surfaces due to preferential nucleation of Sb_2S_3 on the TiO_2 surface has been reported [131]. However, post-deposition annealing at 250 °C, caused noticeable smoothing and changes in the morphology of the crystalline quality of the Sb_2S_3 as revealed in Fig. 14(c) and consequently an increase in the PCE has been reported for Sb_2S_3 solar cells fabricated with SILAR process using 1-D TiO_2 due to annealing effect [25,134].

2.2.3.3. Solvothermal and hydrothermal. In the solvothermal and hydrothermal synthesis of Sb_2S_3 , antimony and sulfide precursors are dissolved in a suitable solvent followed by thermal treatment to form Sb_2S_3 . Aqueous and non-aqueous solvents are used in hydrothermal and solvothermal processes, respectively [135]. These methods are very simple and inexpensive, and the structural properties and morphology can be tuned for structural and morphological optimization by varying the experimental parameters.

Based on the solvothermal route, Kavinchan et al. [136] reported the synthesis of 1-D shuttle-like Sb_2S_3 nanorod-bundles under alkaline conditions (Fig. 15(a)), whereas Sb_2S_3 microbars or different 1-D Sb_2S_3 have been reported by several other research groups [135,137]. As shown in Fig. 15(b), Senthil et al. [135] demonstrated control of the size of the 1-D Sb_2S_3 structure as well as the morphology of the constituent nano-units, in the form of nanorods, dumbbell and sphere by adjusting the temperature and the concentrations of precursor solutions. The amorphous Sb_2S_3 formed at room temperature was observed to grow into irregular nanorods of varying lengths and diameters and then to regular nanorods as a result of solvothermal ripening, which follows an oriented attachment growth mechanism and 1-D growth of Sb_2S_3 was primarily caused by preferential growth of the Sb_2S_3 crystals

along a specific direction owing to the inherently anisotropic and layer-like structure of the Sb_2S_3 crystal.

Several research groups tested Sb_2S_3 thin films fabricated by the solvothermal process for solar cell applications. The reported 1.48% efficiency by Abulikemu et al. [137], for solar cells fabricated with Sb_2S_3 NP synthesized by solvothermal method and Spiro-OMe-TAD as a hole transport layer, is lower than that of similar Sb_2S_3 fabricated by CBD or spin-coated methods. Similarly, Mkawi et al. reported 3.4% efficiency for Mo/ Sb_2S_3 /CdS/ITO/Ag solar cell structure with an open circuit voltage of 451 mV, short circuit current density of 12.47 mA/cm² and, a fill factor of 0.61 [93]. As shown in Fig. 15(c), Mkawi et al. demonstrated the increase in the PEC with the variation of SbCl_3 precursor concentration from 0.75, 0.8, 0.85, and 0.9 mmol, and the observed PCE variation was attributed mainly to an increase in the nucleation and grain size of the Sb_2S_3 film at higher SbCl_3 concentrations (Fig. 15(d)(i)-(iv)). The increase in the grain size was proposed to be caused by Sb crystal lattice deformation, which was attributed to reacting with S atoms during the sulfurization process.

The hydrothermal method, on the other hand, is similar to the solvothermal method, but hydrothermal processes are typically performed under high pressure and at high temperatures to improve Sb_2S_3 properties and to obtain high-quality Sb_2S_3 nanoparticles. The synthesis of various Sb_2S_3 nanostructures with different physical and electrical properties, such as 1-D nanobelt, ribbons, nanowires, nanorods, and nanoneedles has been reported [138–140]. Similarly, Ota et al. reported the synthesis of Sb_2S_3 nanorods using a surfactant-assisted hydrothermal method in which flowerlike morphologies are initially formed due to a heterogeneous nucleation-growth mechanism and these morphologies are then transformed into nanorods via crystal splitting as shown in Fig. 16(a)-(b) [138].

The growth of Sb_2S_3 nanorods by a relatively low-temperature hydrothermal process has been reported by Pal et al. and by using PVP as a capping agent, the shape of Sb_2S_3 was able to modify

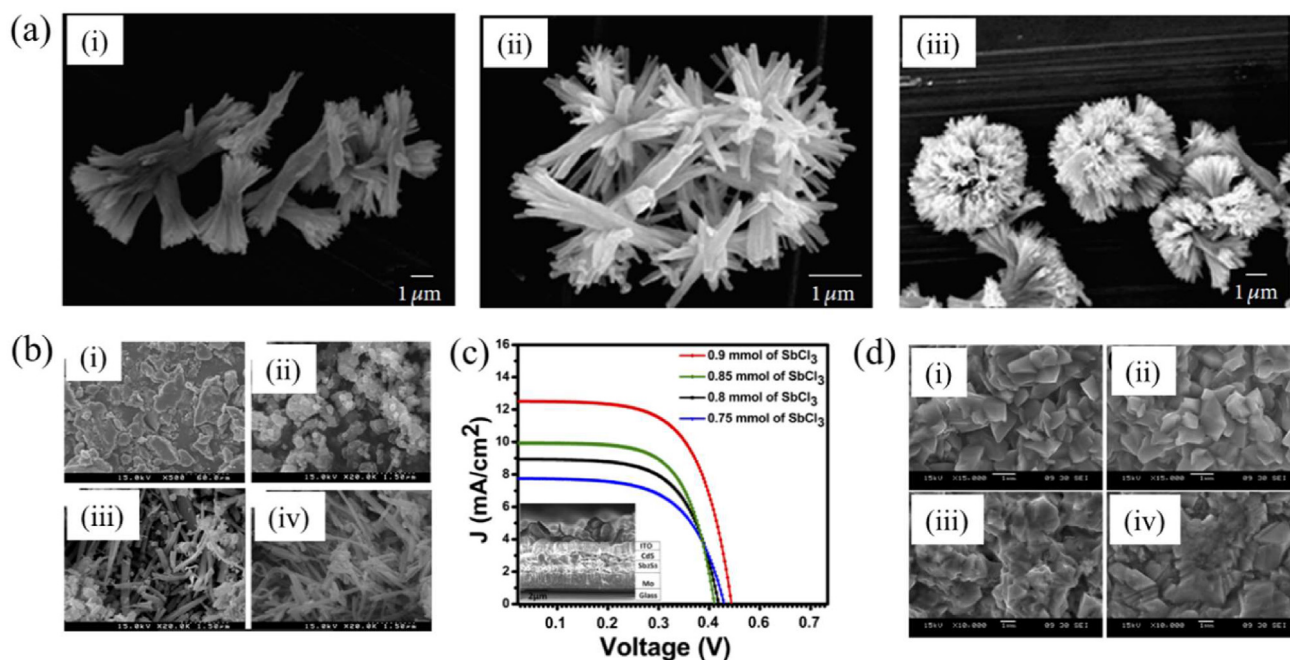


Fig. 15. (a) SEM images of Sb_2S_3 synthesized in ethylene glycol (EG) at (i)–(iii) 120 °C, 140 °C, and 160 °C for 60 min, respectively. Reproduced under terms of the CC-BY license [136], (b) SEM image of Sb_2S_3 nanocrystals synthesized by solvothermal method at (i) 35 °C (ii) 70 °C (iii) 100 °C (iv) 150 °C. Reproduced with permission [135], 2014, Elsevier. (c) J – V characteristics of Sb_2S_3 solar cell devices fabricated using different concentrations of SbCl_3 salt. (d) FE-SEM images of Sb_2S_3 thin films fabricated using different concentrations of SbCl_3 salt of (i) 0.75, (ii) 0.8, (iii) 0.85 and (iv) 0.9 mmol. Reproduced under terms of OSA Open Access Publishing [93].

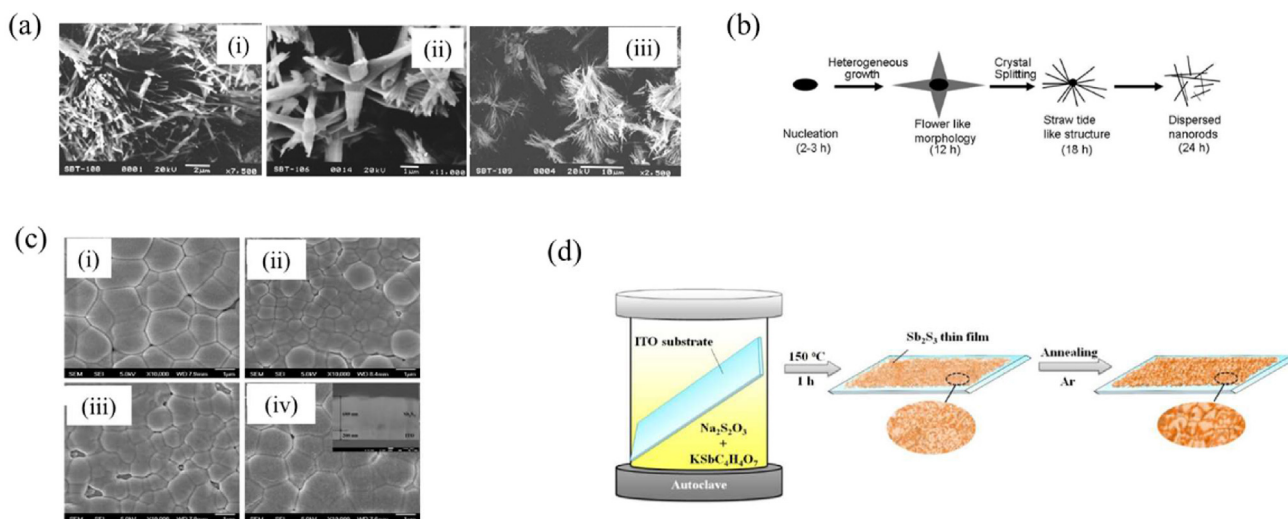


Fig. 16. (a) SEM image of the product obtained after (i) 24 h, (ii) 12 h, (iii) 18 h of reaction duration showing nanorod, flowerlike, and straw tide like morphology respectively. Reproduced with permission [138], 2008, American chemical society. (b) Schematic diagram, depicting possible morphology evolution of Sb_2S_3 from flowerlike morphology to nanorod through a straw tide like structure. Reproduced with permission [138], 2008, American chemical society. (c) SEM images of (i) as-grown Sb_2S_3 film and Sb_2S_3 films annealed at (ii) 250 °C, (iii) 350 °C and (iv) 450 °C; the inset is the cross-section SEM image of Sb_2S_3 film annealed at 450 °C. Reproduced with permission [140], 2016, Elsevier (d) Schematic diagram of the preparation procedures of Sb_2S_3 films. Reproduced with permission [140], 2016, Elsevier.

from nanorods into dumbbell shape structures having different particle sizes and optical properties [139]. As shown in Fig. 16(c)-(d), Liu et al. demonstrated the in-situ deposition of Sb_2S_3 films on the ITO substrate by a hydrothermal process and post-annealing process without the use of complexing agents and the increase in grain size with the increase in the annealing temperature [140]. The Sb_2S_3 films were reported to have a relatively ideal S/Sb atomic ratio, and Sb_2S_3 film annealed at 450 °C exhibited improved optical and electrical performances, with a narrow bandgap of 1.63 eV and low electrical resistivity, indicating that this method will be a promising way to fabricate high-quality Sb_2S_3 films for use as absorber layer materials in solar cells. However, the Sb_2S_3 formed by the hydrothermal process was usually impure, and it was necessary to minimize the incorporation of impurities during the formation Sb_2S_3 . As shown in Fig. 17(a) and (b), Lei et al. demonstrated the fabrication of thin Sb_2S_3 films by the conversion of Sb metal nanoparticles into Sb_2S_3 films on the conducting substrate after reacting with S powder. By in-situ conversion of Sb metal into Sb_2S_3 films on the conductive substrate, it was able to improve the adhesive properties of Sb_2S_3 films onto the substrate and successfully overcome peel off problem generally encountered in the hydrothermally fabricated process.

As reported by several research groups, the solar cell efficiency of Sb_2S_3 films fabricated by the hydrothermal method is not comparable with those similar to other Sb_2S_3 thin film preparation methods, which could be mainly due to the formation of unwanted secondary phases when the hydrothermal reaction is carried at mild conditions. To avoid the formation of secondary phases, Mkawi used a hydrothermal reaction of a solution containing SbCl_3 and $\text{Na}_2\text{S}_2\text{O}_3$ at elevated temperatures, i.e. 200–230 °C, to obtain good quality phase-pure Sb_2S_3 nanobars and reported the increase in PCE as the hydrothermal temperature increased [88]. Mkawi et al. also demonstrated an increase in grain size from 1 μm to 2 μm as the hydrothermal temperature increased from 200 °C to 230 °C and the Sb_2S_3 films formed at high hydrothermal temperatures are dense and without holes or which contributes to the observed higher efficiency, as fewer boundaries enhance the rapid electron conduction and collection.

The main disadvantage of the hydrothermal Sb_2S_3 growth method is that the crystal orientation cannot be precisely controlled

owing to random ion adsorption at the solid–liquid interface. To address this issue, Jin et al. used a “structure-directing” method in which a CdS layer, which acts as nucleation site for the growth of Sb_2S_3 , was prior deposited on the TiO_2 compact layer, followed by the hydrothermal deposition of Sb_2S_3 thin film (Fig. 17(c)) [89]. As CdS acts as a nucleation site for the subsequent growth of Sb_2S_3 , growth of Sb_2S_3 with the preferential orientation of [hk1] has been reported, and an efficiency of 6.4% was observed due to fewer number of grain boundaries and good interfacial contacts with ETL greatly facilitating charge transport and reducing recombination in the device. Instead of CdS seeds, Cd-free Sb_2S_3 planar solar cells have been reported by using In_2S_3 , Sb_2S_3 seed layer, carbon interlayer, metal oxide bilayer, and ZnS layer to improve the quality and adherence of the hydrothermally Sb_2S_3 film [141].

Despite the fact that various Sb_2S_3 structures with different morphologies have been reported in a simple process, the use of different Sb_2S_3 structures fabricated via solvothermal and hydrothermal processes for application in solar cells has not been adequately investigated. On the other hand, it is known that the synthesis of the nanocrystals via solvothermal and hydrothermal processes may lead to form the nanocrystals having defects, especially Sb_2S_3 compounds formed via solvothermal or hydrothermal processes may not be suitable for the application in PVC [139]. Hence more research should be done in order to produce defects-free Sb_2S_3 film by solvothermal or hydrothermal processes. Thin Sb_2S_3 films have also been successfully fabricated using electrochemical, sol–gel, hot injection, and dip coating methods [36,133,137]. Abulikemu reported the formation of urchin-like nanostructure composed of nanorods (NRs) by hot-injection colloidal synthesis of Sb_2S_3 and noted that the diameter of the NRs increased with increasing injection temperature and growth time [137]. By a systematic investigation of the effect of precursors, temperature, and growth time on the formation of Sb_2S_3 NCs, a 1.48% efficiency has been reported for a solar cell fabricated dip coating of Sb_2S_3 NC and spiro-OMe-TAD as a hole conductor.

2.2.4. Advanced chemical methods

In terms of precise controllability of the Sb_2S_3 properties, the common chemical deposition methods described thus far may incapable of ensuring purity, homogeneous surface, required

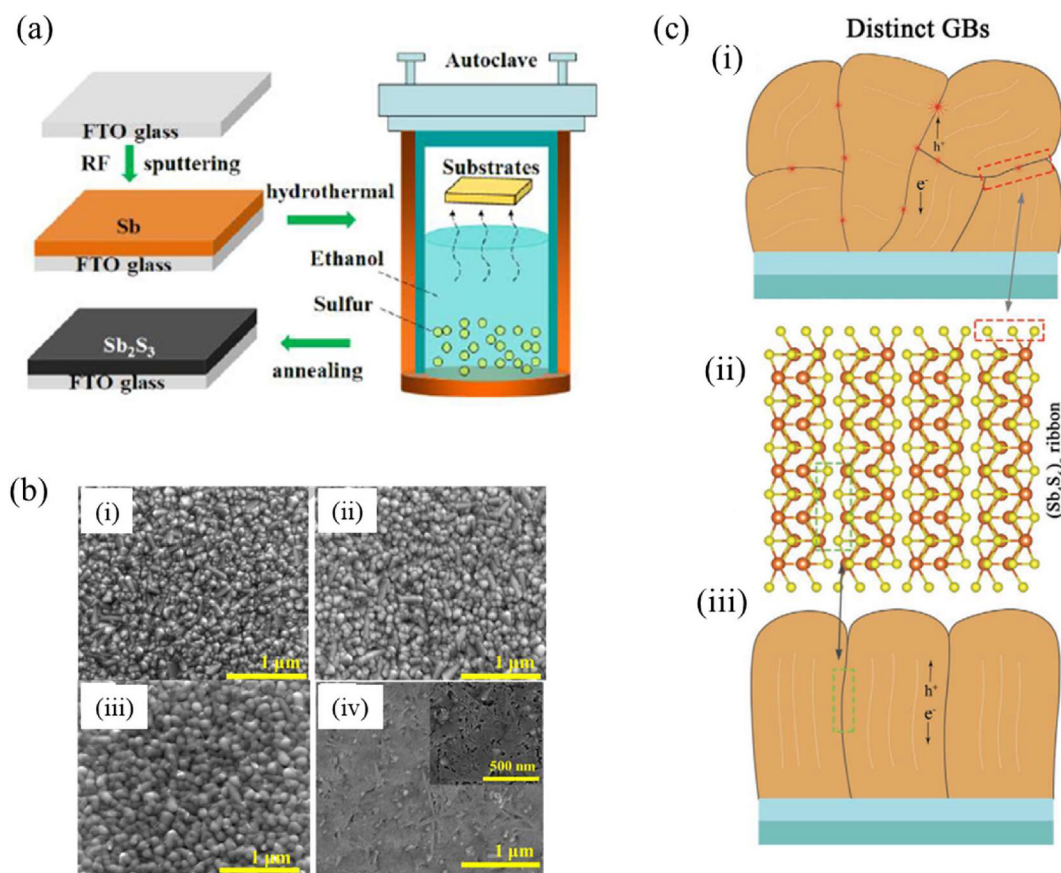


Fig. 17. (a) The schematic of fabricating Sb_2S_3 films. . Reproduced with permission [29], 2018, Elsevier. (b) Surface morphologies of (i) pure FTO, (ii) FTO/Sb, (iii) as-prepared FTO/ Sb_2S_3 and (iv) annealed FTO/ Sb_2S_3 . Reproduced with permission [29], 2018, Elsevier. (c) (i)-(iii) Schematic diagram of distinct grain boundaries in (i) Pn- Sb_2S_3 and (iii) Cd- Sb_2S_3 thin films, Reproduced with permission [89], 2020, wiley-VCH.

thickness, and electrical properties. In general, the low power conversion efficiency and large open-circuit voltage loss have been usually ascribed to interface and bulk extrinsic defects of Sb_2S_3 . Advanced chemical methods, on the other hand, such as chemical vapor deposition (CVD) with low pressure (LPCVD), plasma-enhanced (PECVD), and atomic layer deposition (ALD), have been used to overcome these limitations and obtain highly pure Sb_2S_3 light absorber layers [65].

2.2.4.1. CVD vapor transport. By using aerosol-assisted (AA) CVD, Rodriguez-Castro et al., reported the fabrication of Sb_2S_3 films by thermal decomposition of asymmetric antimony dithiocarbamates, $\text{Sb}[\text{S}_2\text{CN}(\text{Me})\text{R}]_3$ ($\text{R} = \text{Bu}, \text{Hex}, \text{Bz}$), or $\text{Sb}[\text{S}_2\text{COR}]_3$, for $\text{R} = \text{Me}$ (1), Et (2), and Pri (3), under a vacuum to yield high-purity Sb_2S_3 rods. However, the Sb_2S_3 film quality was reported to be dependent on the substrate temperature, and the formation of oxides and mixed oxide/sulfides at higher temperatures was found to be the disadvantage of AA CVD process [142]. Later, the same group used the MOCVD process to deposit Sb_2S_3 thin films using an antimony thiolates $\text{Sb}(\text{SR})_3$ single-source precursor in which R was either Butenol or CH_2CF_3 , and the formation of orthorhombic stibnite Sb_2S_3 films, with stoichiometries in the range $\text{Sb}_2\text{S}_{2.78-3.10}$ has been reported from both precursors [142]. However, the morphologies of the Sb_2S_3 films derived from different precursors were strongly substrate-dependent in which precursor 1 led to the formation of random platelets on both glass and Si substrate, while with precursor 2, growth of uniform Sb_2S_3 films having needle morphology and long rods of stacked platelets have been reported on glass and Si substrate respectively.

On the other hand, as shown in Fig. 18(a)–(d), by AACVD method and with tris(thiobenzoato)antimony(III) complex as a single-source precursor, Murtaza et al. reported the formation of stibnite phase Sb_2S_3 with different morphologies like sheets, thick plates, or bundles of sticks with varying sizes as the deposition temperature increases due to facile transition into different shapes at higher temperatures [65]. Although it has been reported that the fabrication of Sb_2S_3 structures with versatile and different morphologies may be suitable for PVC application, Sb_2S_3 films fabricated by CVD have not been investigated for solar cell applications, which could be due to the instability of single-source antimony complex.

2.2.4.2. ALD. The atomic layer deposition (ALD) technique has been employed to fabricate high-quality Sb_2S_3 thin-absorber films to overcome the disadvantages (i.e. formation of antimony oxides, poor reproducibility, etc.) of conventional chemical methods such as CBD, spin coating methods [69]. As schematically demonstrated by Kim et al. in Fig. 19(a), the main advantage of the ALD method is that the Sb_2S_3 films deposited by ALD have a uniform thickness, and Sb_2S_3 is reported to be free of oxides or oxygen impurities as the ALD process does not include any oxygen sources during the ALD chemical reactions [14]. Furthermore, the ability to precisely control the thickness of Sb_2S_3 was demonstrated by controlling the specific amount of precursors. Consequently, a higher V_{oc} can be expected from the Sb_2S_3 films fabricated by ALD process as deep trap levels that promote charge recombination is absent. Although the ALD method was developed to deposit pure and conformal Sb_2S_3 layers on various substrates, yet to be fully utilized in Sb_2S_3 -based thin film applications.

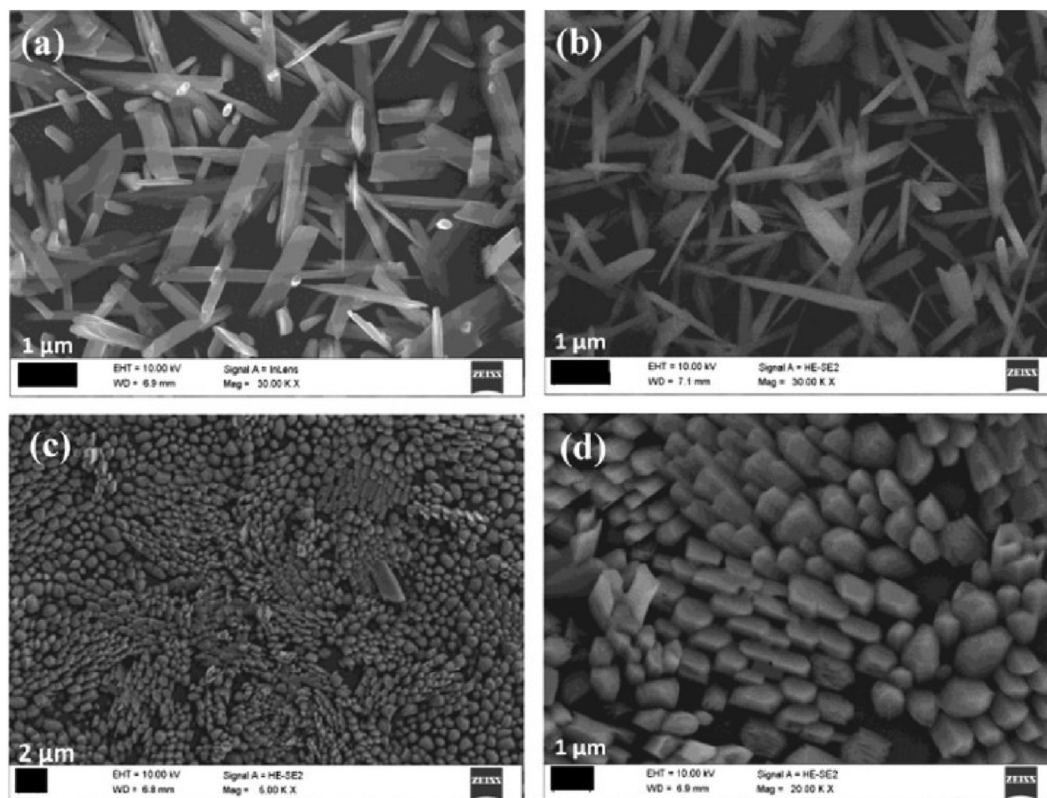


Fig. 18. SEM images of Sb_2S_3 thin films deposited onto glass substrates at (a) 300, (b) 350, and (c) and (d) 400 °C by have been deposited by Aerosol-Assisted Chemical Vapor Deposition (AACVD) from tris(thiobenzoato)antimony(III). Reproduced with permission [65], 2015, Elsevier.

In an attempt to fabricate Sb_2S_3 solar cells by ALD method, Wedemeyer et al. reported an efficiency of up to 2.6% for the solar cell $\text{TiO}_2/\text{Sb}_2\text{S}_3/\text{CuSCN}$ device structure with an optimal Sb_2S_3 thickness of 10 nm [17]. Though the ALD method has been shown to successfully form oxide-free, homogeneously distributed Sb_2S_3 along the depth axis, enhanced efficiencies have not been observed as a result of the structural imperfections in the p-CuSCN deposited by a wet chemical method. On the other hand, Kim et al. reported 5.77% and 2.17% efficiencies for the devices $\text{FTO}/\text{bi-TiO}_2/\text{ALD-Sb}_2\text{S}_3/\text{P3HT}/\text{Au}$ and $\text{FTO}/\text{bi-TiO}_2/\text{CBD-Sb}_2\text{S}_3/\text{P3HT}/\text{Au}$ devices respectively [14]. The improved photovoltaic performance of the device based on ALD- Sb_2S_3 than CBD- Sb_2S_3 has been attributed mainly to the reduced recombination due to the absence of oxides or oxygen impurities as confirmed by XPS analysis. Later, Büttner et al. reported the modification of the Sb_2S_3 layer grown by ALD by deposition of a 1.5 nm ZnS thin layer as an additional interfacial layer for further improvement of diode rectification by passivation of surface defects at the interface to resolve the dewetting issue that occurs on oxide-free Sb_2S_3 material [68]. The presence of the ZnS layer improves the diode rectification of oxide-free- Sb_2S_3 over that of $\text{Sb}_2\text{S}_3\text{O}_x$, and thus the efficiency of solar cells based on ZnS/ Sb_2S_3 material outperforms that of oxide-free Sb_2S_3 . Also, by transient absorption spectroscopy analysis, Büttner et al. were also able to demonstrate that the majority of charge carriers are recombining at the interface between Sb_2S_3 and P3HT, affecting the Voc.

Using alternating exposures of tris(dimethylamino) antimony (TDMASb) and H_2S in a custom-built and modified showerhead viscous flow reactor configuration, Mahuli et al. demonstrated improved conformity of the Sb_2S_3 layer on TiO_2 nanoparticles than the traditional ALD route as shown in HR-TEM image of an ALD grown Sb_2S_3 on TiO_2 nanoparticles at 150 °C (Fig. 19(b)) [38]. However, the reported low PCE of 1.9% with the Spiro-OMeTAD

hole transport layer has been attributed to the reduction of the TiO_2 ETL by the metal–organic precursor during ALD process. In a recent study, Butner et al. investigated the ALD-grown Sb_2S_3 as the absorber material and the effect of the length of TiO_2 NT and Sb_2S_3 loading amount in solid-state heterojunction solar cells to optimize the light absorption while thinning down the light-absorbing layer [69]. The reported higher solar cell performance with a 15 nm thick Sb_2S_3 layer than that of a 5 nm thick layer in planar cell and higher solar performance with a 5 nm thick Sb_2S_3 layer than that with a 15 nm thick layer in 1-D structures was mainly attributed to dewetting effect. As demonstrated schematically in Fig. 19(c) and SEM image (Fig. 19(d)), during the crystallization process, the aggregation of larger Sb_2S_3 led to the generates discontinuous rod-like structures shaped by the TiO_2 nanochannel due to dewetting while the with a 5 nm Sb_2S_3 thick layer, such a damaging dewetting has not been observed. However, the reported solar cell efficiency for Sb_2S_3 with 1-D TiO_2 was inferior to that of the planar cell indicates that the vapor deposition method is preferable to obtain a more homogeneous Sb_2S_3 film surface in the planar device than 1-D structure.

2.3. Physical methods

Physical deposition methods such as evaporation and sputtering are preferred over chemical deposition methods for obtaining high-quality Sb_2S_3 thin films for device applications. The vacuum thermal evaporation technique, electron beam evaporation, pulsed laser deposition and direct/current/radio frequency magnetron sputtering are the most commonly reported physical methods for fabricating Sb_2S_3 thin films in solar cell applications. Physical evaporation is usually done under controlled atmospheric conditions or in a vacuum, in which materials are converted from the

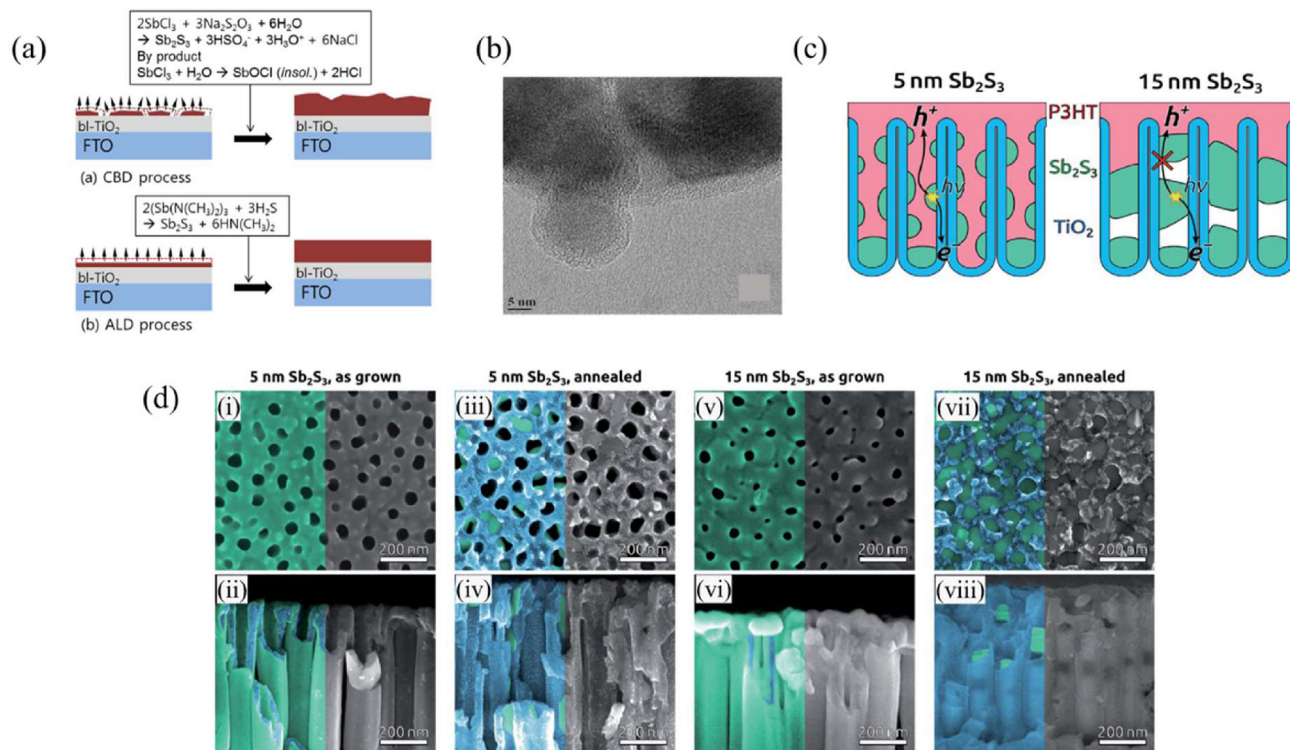


Fig. 19. (a) Schematic illustration for the formation of Sb₂S₃ thin-layer on the bi-TiO₂/FTO substrate by CBD and ALD process. [14], 2014, Royal Society of Chemistry. (b) HR-TEM imaging revealing an excellent conformity of ALD grown a-Sb₂S₃ on TiO₂ nanoparticles at 150 °C. Reproduced with permission [38], 2020, American Institute of Physics. (c) Schematic cross-section of a TiO₂ NT solar cell with 15 nm and 5 nm of Sb₂S₃. Reproduced under terms of the CC-BY license [69]. (d) SEM top views (i, iii, v and vii) and cross-sections (ii, iv, vi and viii) of TiO₂ NTs with Sb₂S₃ ALD layers before and after annealing with TiO₂ and Sb₂S₃ indicated in blue and green, respectively. (i and ii) 15 nm of Sb₂S₃ as grown, (iii and iv) 15 nm of Sb₂S₃ crystallized, (v and vi) 5 nm of Sb₂S₃ as grown, (vii and viii) 5 nm of Sb₂S₃ crystallized. Reproduced under terms of the CC-BY license, [69].

solid phase to the vapor phase and then back to the solid phase on the substrate. Although physical methods for producing thin films enable the production of precise, controlled, and high-quality Sb₂S₃, they are not cost-effective.

2.3.1. Vacuum thermal evaporation

It has been reported that the properties of thin films fabricated by vacuum thermal evaporation are highly dependent on the material properties and the applied potential to the substrate under vacuum. A solar cell with a device structure of FTO/CdS/Sb₂S₃/C–Ag, in which Sb₂S₃ film was prepared using the thermal evaporation technique reported by Escorcia-García, has a Voc of 600 mV, a Jsc of 6.1 mA/cm², and a solar energy conversion efficiency of 1.27% [94]. Because no improvement in the crystalline grains was observed using a thermal evaporation method, the reported efficiency was found to be even lower than that of a chemically fabricated Sb₂S₃ thin film with a similar device structure. Later, Mayon et al. reported that the Sb₂S₃ deposited by the thermal evaporation method was sulfur-rich, and thus the mean coordination number is lower than the stoichiometric Sb₂S₃ deposited by the solution-based process because sulfur evaporates more easily than antimony. Consequently, during the post-deposition annealing step, it has been reported the flattening of the malleable Sb₂S₃ leads to the deposition of a thin and uniform hole transport layer as shown in Fig. 20(a) [50]. Additionally, Sb₂S₃ films fabricated by the thermal evaporation method was reported to have better electronic properties due to the presence of a high proportion of (211), (221), (041), and (141) crystal planes, and a low proportion of the (020) crystal plane. By the co-evaporation of sulfur or antimony during thermal evaporation of Sb₂S₃, Yin et al. reported that the PCE of Sb₂S₃ films fabricated by thermal evaporation can be enhanced

under sulfur-rich conditions while the decrease in PCE has been reported under antimony-rich condition due to change in the carrier concentration and transport dynamics [100].

Though it is possible to produce homogeneous Sb₂S₃ films by a thermal process, one of the most common issues with Sb₂S₃ deposition in the thermal process is the poor thermal stability of Sb₂S₃ in a vacuum, which results in significant compositional deviation, limiting the ability to achieve high-quality Sb₂S₃ crystalline films [50]. Hence, Wang et al. used a selenization-based post-treatment approach and found that the post-selenization of Sb₂S₃ resulted in increased crystallinity and the formation of micron-sized large grains, thereby promoting grain growth, as evidenced by the SEM images shown in Fig. 20(b) [98]. It has also been reported that the existence of a gradient composition of Sb₂S₃/Sb₂S₃(Se)/Sb₂Se₃ (Fig. 20(c)) due to partial S atom replacement of S atoms by Se atoms at the interface could improve photogenerated positive carrier transport from the p–n junction to the anode. On the other hand, Lan et al. employed a different approach to improve the PCE of thermally evaporated Sb₂S₃ films-based solar cells, in which they used the Li-doped TiO₂ films to improve electron extraction and transport properties, and a PCE of 1.79% and 4.04%, were reported for TiO₂ and Li-doped TiO₂ films respectively [12].

In a similar way to thermal evaporation, Yuan et al. reported the use of the rapid thermal evaporation (RTE) method to deposit compact Sb₂S₃ films at a much faster rate than regular thermal evaporation, in which the source was melted and then evaporated at liquid phase [95]. In their study, Yuan et al. reported that increasing the evaporation temperature from 500 to 550 °C increased the grain size from 200 to 500 nm due to increased fusion of the grain boundary together and higher Sb₂S₃ vapor pressure at higher temperatures (Fig. 21(a)). Additionally, the use of the fast-

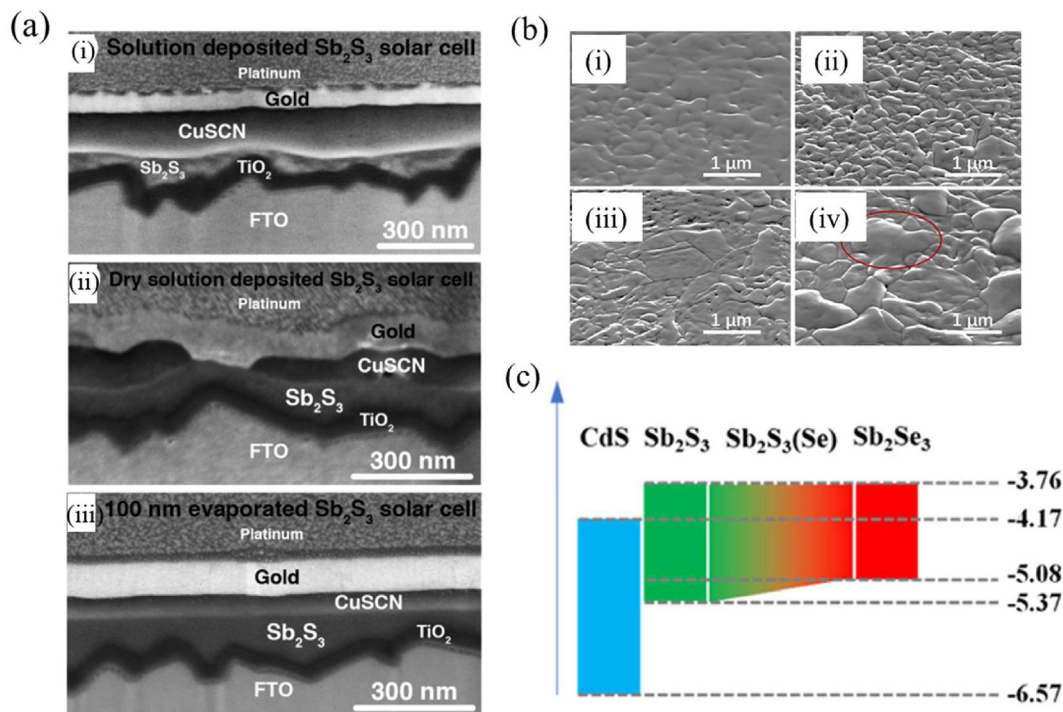


Fig. 20. (a) Cross-section images of the antimony sulphide solar cells obtained with an SEM-FIB system. Note that the platinum layer was deposited on top of the gold contact to prevent damage to the sample from the FIB milling process. Reproduced with permission [50], 2015, Wiley-VCH. (b) Top-view SEM images of Sb_2S_3 films under various treatment conditions. (i) Untreated, (ii) Vacuum annealed, (iii) selenization for 15 min, (iv) Selenization for 20 min. Reproduced under terms of the CC-BY license [98]. (c) energy levels along the vertical depth of selenization Sb_2S_3 film. Reproduced under terms of the CC-BY license, [98].

cooling process resulted in improved electronic properties due to preferential growth of the (120) phase and suppression of the (200) phase of Sb_2S_3 (Fig. 21(b)). A highly stable solar cell with a PCE of 3.5% has been reported for the optimized planar solar cells based on ITO/CdS/ Sb_2S_3 /Au by growing high-quality Sb_2S_3 thin film by the RTE method and avoiding the use of oxide ETL and common HTL to address the discoloration effect and degradation of HTL. The same group reported that Se post-treatment of Sb_2S_3 deposited by RTE method increased the PCE of ITO/CdS/ Sb_2S_3 /Au to 4.17% as a result of interface and bulk defect passivation as well as an increase in the VB maximum [47].

However, the formation of horizontally stacked [120] Sb_2S_3 by the RTE method led to diminished J_{sc} as the electrons needed to hop between the ribbon layers and was found to be the main reason for the reported low PCE of solar cells fabricated with the Sb_2S_3 films on CdS [47,87]. Hence, Zeng et al. [87] adopted the VTD method, which is a modification of the RTD method to stack the Sb_2S_3 film vertical [hk1] orientation on CdS. As shown in Fig. 21(c), Sb_2S_3 deposited on CdS by VTD had mostly [121] and [221] orientations, whereas RTE- Sb_2S_3 reported having [120] and [200] orientations [87] (Fig. 21(d)). They reported a PCE of 4.73% and a J_{sc} of 15.6 mA/cm^2 for (ITO)/CdS/ Sb_2S_3 /Au, which has been mainly attributed to the improved J_{sc} resulting from the orientated film, which improves carrier transport, as well as the higher grain size of the Sb_2S_3 film fabricated by the VTD method.

Later, Deng et al. reported the RTE deposition of Sb_2S_3 and noted the formation of large Sb_2S_3 grains on TiO_2 ETL at a relatively lower crystalline temperature of 300 °C compared to the 500 °C crystallization temperature required to grow a similar size Sb_2S_3 grain on CdS by the RTE method [28,143]. The solar cell performance of a planar device fabricated with FTO/ TiO_2 / Sb_2S_3 /Au without HTM layer was reported to increase from 0.91 to 2.48% when the increase of crystalline temperature from 200 °C to 300 °C as a result of the

growth of larger Sb_2S_3 grains via Ostwald ripening and the formation of a smooth and compact Sb_2S_3 surface. Further temperature increases to 320 °C have been shown to have a negative effect on PCE due to the formation of pinholes. The PCE efficiency was reported to increase by 3.2% after further annealing the Sb_2S_3 films deposited by the RTE method in the Se atmosphere, with the improved PCE efficiency attributed to the formation of larger grain sizes and clearer grain boundaries in Se annealed Sb_2S_3 than in as-deposited Sb_2S_3 . Furthermore, it has been also reported the enhancement of the rectification factor in Se-treated Sb_2S_3 film compared to that of as-deposited Sb_2S_3 film. Similarly, Pan et al. reported the deposition of the Sb_2S_3 thin film by the RTE and the fabrication of solar cell of the structure Soda-lime glass (SLG)/Mo/ Sb_2S_3 /CdS/iZO/AZO/Ni:Al and found that the film quality, and hence the PCE can be improved by optimizing the substrate temperature and evaporation time as it can be manipulated to obtain desired film crystallization and the grain size [99].

To mitigate the interface defects and transport loss, Deng et al. reported the quasi-epitaxial growth of vertically orientated Sb_2S_3 layer on FTO/ TiO_2 by the RTE method [143]. It is a known fact that in terms of efficient charge collection and light trapping of Sb_2S_3 films, vertical [hk1] orientation is preferred over the parallel [hk0] orientation to the TiO_2 ETL [143]. However, due to randomly distributed crystal facets of the TiO_2 substrate, Sb_2S_3 was found to grow along with its preferred low energy [hk0] orientation spreading all over the TiO_2 resulting in nonideal interchain hopping style carrier transport (Fig. 21(e)i). However, vertically stacked Sb_2S_3 alone in the [001] orientation on lattice-mismatched TiO_2 has been shown to increase interface charge recombination (Fig. 21(e)ii). Hence, Deng et al. tuned the TiO_2 exposure facets by the thermal treatment in which oxygen vacancy V_o is created in TiO_2 for lattice-matched epitaxial growth for Sb_2S_3 alone [001] orientation to promote charge carrier transport as shown in Fig. 21(e)iii. As

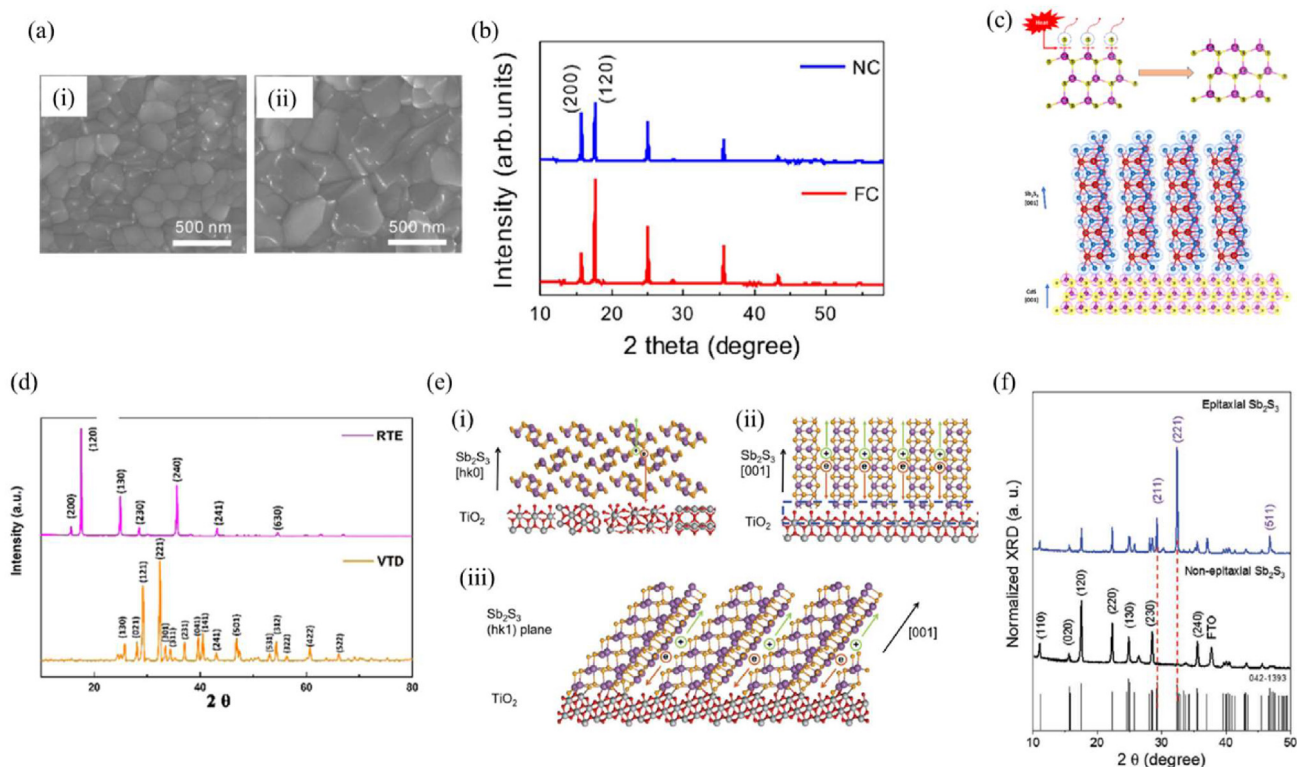


Fig. 21. (a) Top view SEM images of Sb_2S_3 solar cells (i) (Lower crystallization temperature, 500°C) LT- Sb_2S_3 device, (ii) (Higher crystallization temperature, 550°C) HT- Sb_2S_3 device. Reproduced with permission [95], 2016, Elsevier. (b) XRD patterns of FC- Sb_2S_3 and NC- Sb_2S_3 thin film. Reproduced with permission [95], 2016, Elsevier. (c) Cd-S bond breakage and the adsorption of Sb_2S_3 molecules onto Cd^{2+} dangling bonds exposed to CdS surface during the vapor transport deposition (VTD) process. Reproduced with permission [87]. (d) XRD patterns of the rapid thermal evaporation (RTE) and VTD samples. Reproduced with permission [87], 2020, American Chemical Society (e) Crystal structures of $(\text{Sb}_4\text{S}_6)_n$ ribbons schematically stacked on TiO_2 . (i) $[\text{hk}0]$ orientation Sb_2S_3 ribbons lie on TiO_2 nanoparticle substrate and the photocarriers transport in a hopping style. (ii) $[001]$ orientation Sb_2S_3 ribbons directly stand on crystalline TiO_2 with mismatched lattices. (iii) $[\text{hk}1]$ orientation Sb_2S_3 ribbons chemically bond with crystalline $[101]$ TiO_2 surface [143], 2019, Wiley-VCH. (f) XRD spectra of Sb_2S_3 films from epitaxial and nonepitaxial growth. Reproduced with permission [143], 2019, Wiley-VCH.

demonstrated in XRD analysis (Fig. 21(f)), the nonepitaxial growth preferred $[120]$ orientation while epitaxial growth preferred $[221]$ and $[211]$ orientation. Hence, Deng et al. reported a stable 5.4% efficient solar cell for epitaxial growth and optimized Sb_2S_3 grain size, and the enhanced PCE was attributed to light trapping effects, improved p-n junction quality and higher built-in-potential. Similarly, Ishaq et al., reported a PCE of 5.16% and a record V_{OC} of 702 mV for an epitaxial growth film and full-inorganic Sb_2S_3 by the RTE method on Zn incorporated TiO_2 [144], and the enhanced performance was attributed to the formation of compact, highly crystalline, and uniform film with a large grain size of Sb_2S_3 on Zn incorporated TiO_2 , improving the junction quality by suppressing the interface recombination and reverse saturation current.

2.3.2. Sublimation and radio frequency sputtering (RF sputtering)

The sublimation and radio frequency sputtering (RF) deposition methods are preferable in the planar film system to achieve a more homogeneous film and to obtain large crystal grains due to the fast deposition process [12,31]. In the deposition of Sb_2S_3 film by sublimation, the saturated Sb/S vapor produced by heating Sb_2S_3 was condensed to form films on the substrate in the cold area [145]. PCEs of 3.08 and 1.38% have been reported for the Sb_2S_3 film deposited on TiO_2 and CdS substrate, respectively, using rapid sublimation of Sb_2S_3 with a short deposition time under 30 s [145]. The reported Sb_2S_3 grain sizes on TiO_2 and CdS substrates were 500 nm and 200–500 nm, respectively, and the increased PCE on TiO_2 over CdS substrate has been attributed to the formation of larger crystal Sb_2S_3 grains, resulting in longer diffusion lengths for the electrons and holes pairs. By manipulating the substrate and

source temperatures, Guo et al. demonstrated the formation of nearly $1\ \mu\text{m}$ large Sb_2S_3 grains on the CdS substrate and a 3.8% PCE has been reported with the configuration of glass/FTO/CdS/ Sb_2S_3 /graphite back contact [146]. The observed higher PCE with Sb_2S_3 /CdS by Guo et al. [146], can be attributed to the formation of larger Sb_2S_3 grains than that of smaller crystal grains reported by Zeng et al. [145]. The as-grown Sb_2S_3 film has been reported to have a strong (211) -preferred orientation benefitting the charge transfer along with the $(\text{Sb}_4\text{S}_6)_n$ ribbons in the Sb_2S_3 film. Based on the first-principles density functional theory (DFT) study, they predicated the p-type nature owing to S-on-Sb antisites (SSb) and the limitation of the device performance by the S vacancies, and they proposed further improvement by controlling the S environment during film deposition or through post-deposition sulfurization. The deposition of Sb_2S_3 thin films on the FTO substrate via magnetron sputtering of an Sb_2S_3 target has been reported by Gao et al. [146] and the increase in the grain size and hence consequent enhancement in the PCE for the Sb_2S_3 deposited RF has been reported due to increase in the grain size with the post-annealing temperature. By doping of elemental Cu into Sb_2S_3 films prepared by RF magnetron sputtering, the increase in the electronic carrier concentration from 6.28×10^9 to $6.06 \times 10^{10}\ \text{cm}^{-3}$ and also the uplifting of the Fermi level has been reported by Lei et al. [90]. The increase in built-in potential due to improved carrier concentration, combined with the up-shift of the Fermi level of RF-sputtered Sb_2S_3 films, may boost the photovoltaic performance of solar cells. Similarly, post-sulfurization or post-selenization of RF sputtered Sb_2S_3 films resulted in a highly crystalline thin film with large crystal grains an improvement in PCE performance [51].

3. Prospective and summary: challenges and opportunities for the future research

The effect of morphology and structural changes in Sb₂S₃ films fabricated using various thin film fabrication methods on solar cell performance was reviewed. The review discusses the fundamental structure and properties of Sb₂S₃, and then demonstrates how the morphology and structural changes of Sb₂S₃ films produced using various fabrication techniques and parameters affect solar cell performance. This study also includes significant recent developments and current research trends of Sb₂S₃-based photovoltaic devices paving a new path to improving Sb₂S₃ performance in the future.

The orthorhombic Sb₂S₃ fabricated by various chemical or physical methods generally has finite (Sb₄S₆)_n ribbon-like structures along the c-axis. The bandgap of Sb₂S₃ has been reported to vary in the range of 1.56–2.25 eV, while the reported conductivity of Sb₂S₃ in room temperature is 10⁻⁸ – 10⁻⁹ Ω⁻¹cm⁻¹ depending on the fabrication methods and the parameters. The chemical bath deposition method is the most commonly used thin-film Sb₂S₃ fabrication technique due to its simplicity and ease of fabrication. However, Sb₂S₃ films formed by the CBD method is an amorphous in nature, the films required an additional temperature treatment with air/inert gas conditions to optimize the crystalline properties of Sb₂S₃. One of the major disadvantages of the conventional chemical bath deposition method is that the thickness of Sb₂S₃ film deposition does not depend linearly on reaction time because Sb₂S₃ deposition is dependent on nucleation in the heterogeneous solution and growth process. Furthermore, it has been reported that the formation of antimony oxides during the deposition of Sb₂S₃ has a negative impact on device performance, which has been partially eliminated by using gaseous sulfur during the deposition process. On the other hand, the ALD method can control the thickness and morphology of Sb₂S₃ thin films much more precisely than the CBD method. The significantly improved control of thickness, morphology (denser), and phase purity in the films deposited by ALD resulted in enhanced solar cell performance. The purity of the Sb₂S₃ absorber layer deposited by the chemical spray pyrolysis (CSP) method is determined by the precursor solution, composition ratio with a Sb/S ratio greater than 1:3 yielding an oxide-free Sb₂S₃ layer. The thermal evaporation method of Sb₂S₃ has many advantages, including being simple and low-cost, using a non-vacuum technique, and making large-area solar cell deposition feasible rather than chemical bath deposition (CBD). Although the higher temperature requirement of the thermal evaporation method of Sb₂S₃ deposition produces sulfur defects, the trap states produced result in inferior solar cell performance. The electrodeposition method is a simple, low-cost method that allows for better composition control and uniformity. However, the electrodeposited films, have a high resistivity and a thin film thickness. On the other hand, vacuum-based synthesis techniques can render denser, higher purity, and larger-grained films. The Sb₂S₃ Layers deposited at higher temperatures (550 °C) were compact and composed of large grains (500 nm).

In general, Sb₂S₃-based solar cells do not perform as well as other thin-film-based solar cells. The highest reported efficiency ~8% (with an average V_{oc}, J_{sc} and FF of in the range 400–600 mV, 12–18 mA/cm² and 50–60% respectively) for Sb₂S₃ solar cells in planar configuration is far behind the projected PCE efficiency of ~28% (with J_{sc} = 22.46 mA/cm², V_{oc} = 1.402 V, FF = 91%) under an AM 1.5G spectral irradiance for single p–n junction with an absorber of 1.7 eV. When compared to theoretical calculations, the experimentally observed low V_{oc} and low FF values for Sb₂S₃ solar cells could be the primary cause of poor solar performance. The reported poor performance of Sb₂S₃ in solar devices implies that

significant factors such as intrinsically formed traps and the presence of surface defect states, which have been identified as limiting factors for device performance, have not been successfully addressed by the present film fabrication methods.

Although the ability to manipulate the optical and electrical properties, as well as the morphology of Sb₂S₃ films, has been demonstrated using chemical or physical Sb₂S₃ film fabrication methods, these films require an additional temperature treatment with air/inert gas conditions to optimize the crystalline properties of Sb₂S₃. Significantly, while various Sb₂S₃ films fabricated using different processes were found to be suitable for solar cell applications as a light-harvesting material, all of them were found to contain defects, which may be related to the reported low PCE. As a result, it's critical to look for alternative ways to overcome these flaws, not just by changing the fabrication method. One important factor is that the effect of oxygen during the fabrication of Sb₂S₃ films by various methods should be seriously considered, as the literature indicates significant positive as well as negative effects of oxygen during fabrication. Despite the fact that oxygen plays a critical role in the fabrication and deposition of Sb₂S₃, its precise role in device performance is unknown. An investigation into the critical role of oxygen in Sb₂S₃ fabrication may result in a streamlining of the Sb₂S₃ fabrication method as well as the desired conductivity type and conductivity, which may overcome the current efficiency bottleneck of Sb₂S₃-based solar cells.

Achieving the target of a 28% efficient Sb₂S₃ solar cell is a significant challenge, with critical issues like absorber and interfacial properties necessitating careful optimization. The morphology of Sb₂S₃ needs to be carefully tuned to obtain defect-free (or with minimum defects) large grain size and high crystalline Sb₂S₃ films as minority carrier lifetime, buffer/absorber interface recombination, tunneling enhanced recombination, and recombination due to bulk defects have been identified theoretically as the major loss mechanisms. On the other hand, achieving the goal of a 28% efficient Sb₂S₃ solar cell is a significant challenge due to the large gap between the theoretical predicted and current record Sb₂S₃ device PCE, which necessitates a large number of comprehensive research efforts. However, the lack of such coordinated studies could be one of the reasons for the slow progress on Sb₂S₃ solar cells. Finally, given the recent interest in low-cost earth abundant materials for solar cell applications, advances in Sb₂S₃ thin film fabrication technology may result in better Sb₂S₃ film quality and device performance.

4. Conclusion

In this review, the fundamental properties of Sb₂S₃, as well as structural and morphological changes caused by various techniques, were covered. Sb₂S₃ is a unique compound with a single-phase, anisotropic crystal structure, high absorption coefficient, stability, and wide bandgap (~1.7 eV). Despite reported higher efficiencies for sensitized Sb₂S₃ Solar cells, the planar device structure is more competitive for Sb₂S₃-based solar cells. The spin coating technique is the most common and suitable method for planar structure, and the current efficiency of such a cell in a configuration of FTO/compact-TiO₂/Sb₂S₃/SbCl₃/Spiro-OMeTAD/Au reached an efficiency of 6.9%. The high density of interface defects and poor carrier transport are the limitation of Sb₂S₃ based solar cells are. Synthesis conditions and surface treatments methods were reviewed in this paper to improve the Sb₂S₃ based thin-film solar cells. The most suitable temperature of crystallinity of Sb₂S₃ is recorded as 300 °C in inert gas. Surface treatments like sulfurization and selenization are temperature and time-sensitive. With the sulfurization technique, the Sb₂S₃ sensitized solar cells reached the highest efficiency of 7.5%. Large Sb₂S₃ grains with high

crystallinity are one of the critical factors that enhance the recombination resistance and lead to the device's performance. By utilizing proper conditions of Sb₂S₃ fabrication, high-quality films can be produced, which is suitable for thin-film solar cell applications. Hence, it is critical to look for novel ways to fabricate thin Sb₂S₃ films in order to break through the current PCE limits and lead to the utilization of earth-abundant and harmless Sb₂S₃ in the future.

Author contributions

The manuscript was written through the contributions of all authors. Jayasundera Bandara: Conceptualization, Writing-Reviewing and Editing, Arumukham Manjeevan: Editing and writing, Mohaiyadeen Aliyar Farhana: Editing and writing. All authors have given approval to the final version of the manuscript.

Declaration of Competing Interest

There are no conflicts to declare.

Acknowledgment

Financial support from the National Research Council of Sri Lanka (Grant 18-005) is highly appreciated.

References

- [1] D. Gielen, F. Boshell, D. Saygin, M.D. Bazilian, N. Wagner, R. Gorini, The role of renewable energy in the global energy transformation, *Energy Strategy Rev.* 24 (2019) 38–50.
- [2] Y. Chang, J. Lee, H. Yoon, Alternative projection of the world energy consumption-in comparison with the 2010 international energy outlook, *Energy Pol.* 50 (2012) 154–160.
- [3] A. Jäger-Waldau, Snapshot of photovoltaics-february 2020, *Energies* 13 (2020) 930.
- [4] R. Kondrotas, C. Chen, J. Tang, Sb₂S₃ solar cells, *Joule* 2 (2018) 857–878.
- [5] J. Ramanujam, U. Singh, Copper indium gallium selenide based solar cells – Review, *Energy Environ. Sci.* 9 (2017).
- [6] P.P. Boix, Y.H. Lee, F. Fabregat-Santiago, S.H. Im, I. Mora-Sero, J. Bisquert, S.I. Seok, From flat to nanostructured photovoltaics: balance between thickness of the absorber and charge screening in sensitized solar cells, *ACS Nano* 6 (2011) 873–880.
- [7] M. Gloeckler, I. Sankin, Z. Zhao, CdTe solar cells at the threshold to 20% efficiency, *IEEE J. Photovoltaics* 3 (2013) 1389–1393.
- [8] Y. Hirai, Y. Kurokawa, A. Yamada, Numerical study of Cu(In,Ga)Se₂ solar cell performance toward 23% conversion efficiency, *Jpn. J. Appl. Phys.* 53 (2013), 012301.
- [9] A. Mavlonov, T. Razykov, F. Raziq, J. Gan, J. Chantana, Y. Kawano, T. Nishimura, H. Wei, A. Zakutayev, T. Minemoto, X. Zu, S. Li, L. Qiao, A review of Sb₂Se₃ photovoltaic absorber materials and thin-film solar cells, *Sol. Energy* 201 (2020) 227–246.
- [10] M. Aliyar Farhana, J. Bandara, Enhancement of the photoconversion efficiency of Sb₂S₃ based solar cell by overall optimization of electron transport, light harvesting and hole transport layers, *Sol. Energy* 247 (2022) 32–40.
- [11] Y.C. Choi, D.U. Lee, J.H. Noh, E.K. Kim, S.I. Seok, Highly improved Sb₂S₃ sensitized-inorganic-organic heterojunction solar cells and quantification of traps by deep-level transient spectroscopy, *Adv. Funct. Mater.* (2014) n/a.
- [12] C. Lan, J. Luo, H. Lan, B. Fan, H. Peng, J. Zhao, H. Sun, Z. Zheng, G. Liang, P. Fan, Enhanced charge extraction of Li-doped TiO₂ for efficient thermal-evaporated Sb₂S₃ thin film solar cells, *Materials* 11 (2018) 355.
- [13] J.A. Christians, P.V. Kamat, Trap and transfer. Two-step hole injection across the Sb₂S₃/CuSCN interface in solid-state solar cells, *ACS Nano* 7 (2013) 7967–7974.
- [14] D.-H. Kim, S.-J. Lee, M.S. Park, J.-K. Kang, J.H. Heo, S.H. Im, S.-J. Sung, Highly reproducible planar Sb₂S₃-sensitized solar cells based on atomic layer deposition, *Nanoscale* 6 (2014) 14549–14554.
- [15] J. Zhong, X. Zhang, Y. Zheng, M. Wen, S. Wu, J. Gao, X. Gao, J.-M. Liu, H. Zhao, High efficiency solar cells as fabricated by Sb₂S₃-modified TiO₂ nanofibrous networks, *ACS Appl. Mater. Interfaces* 5 (2013) 8345–8350.
- [16] T. Englman, E. Terkieltaub, L. Etgar, High open circuit voltage in Sb₂S₃/metal oxide-based solar cells, *J. Phys. Chem. C* 119 (2015) 12904–12909.
- [17] H. Wedemeyer, J. Michels, R. Chmielowski, S. Bourdais, T. Muto, M. Sugiura, G. Dennler, J. Bachmann, Nanocrystalline solar cells with an antimony sulfide solid absorber by atomic layer deposition, *Energy Environ. Sci.* 6 (2013) 67–71.
- [18] E. Zimmermann, T. Pfadler, J. Kalb, J.A. Dorman, D. Sommer, G. Hahn, J. Weickert, L. Schmidt-Mende, Toward high-efficiency solution-processed planar heterojunction Sb₂S₃ solar cells, *Adv. Sci.* 2 (2015), 1500059.
- [19] J. Li, X. Liu, J. Yao, The enhanced photovoltaic performance of Sb₂S₃ solar cells by thermal decomposition of antimony ethyl xanthate with thiourea doping, *Energy Technol.* 8 (2020), 1900841.
- [20] S.H. Im, H.-j. Kim, J.H. Rhee, C.-S. Lim, S.I. Seok, Performance improvement of Sb₂S₃-sensitized solar cell by introducing hole buffer layer in cobalt complex electrolyte, *Energy Environ. Sci.* 4 (2011) 2799–2802.
- [21] S.-J. Moon, Y. Itzhaik, J.-H. Yum, S.M. Zakeeruddin, G. Hodes, M. Grätzel, Sb₂S₃-Based mesoscopic solar cell using an organic hole conductor, *J. Phys. Chem. Lett.* 1 (2010) 1524–1527.
- [22] R.A. Miranda Gamboa, O.A. Jaramillo-Quintero, Y.A. Alarcón Altamirano, M.O. Concha-Guzmán, M.E. Rincón, A novel nanocomposite based on NiOx-incorporated P3HT as hole transport material for Sb₂S₃ solar cells with enhanced device performance, *J. Colloid Interface Sci.* 535 (2019) 400–407.
- [23] L. Zhang, C. Jiang, C. Wu, H. Ju, G. Jiang, W. Liu, C. Zhu, T. Chen, V2O5 as hole transporting material for efficient all inorganic Sb₂S₃ solar cells, *ACS Appl. Mater. Interfaces* 10 (2018) 27098–27105.
- [24] Y. Liang, X. Zhong, H. Song, Y. Zhang, D. Zhang, Y. Zhang, J. Wang, Study of photovoltaic performance of Sb₂S₃/CdS quantum dot co-sensitized solar cells fabricated using iodine-based gel polymer electrolytes, *Appl. Phys. A* 124 (2018).
- [25] Y. Li, L. Wei, R. Zhang, Y. Chen, L. Mei, J. Jiao, Annealing effect on Sb₂S₃-TiO₂ nanostructures for solar cell applications, *Nanoscale Res. Lett.* 8 (2013) 1–7.
- [26] F. Giordano, A. Abate, J.P. Correa Baena, M. Saliba, T. Matsui, S.H. Im, S.M. Zakeeruddin, M.K. Nazeeruddin, A. Hagfeldt, M. Graetzel, Enhanced electronic properties in mesoporous TiO₂ via lithium doping for high-efficiency perovskite solar cells, *Nat. Commun.* 7 (2016), 10379.
- [27] W. Chen, L. Jiang, R. Pathak, F. Wu, Sb₂S₃/TiO₂ heterojunction solar cells based on carbon electrode with higher photocurrent, *ECS J. Solid State Sci. Technol.* 8 (2019) Q67–Q71.
- [28] H. Deng, S. Yuan, X. Yang, F. Cai, C. Hu, K. Qiao, J. Zhang, J. Tang, H. Song, Z. He, Efficient and stable TiO₂/Sb₂S₃ planar solar cells from absorber crystallization and Se-atmosphere annealing, *Mater. Today Energy* 3 (2017) 15–23.
- [29] H. Lei, T. Lin, X. Wang, S. Zhang, Q. Cheng, X. Chen, Z. Tan, J. Chen, A novel in situ hydrothermal preparation route for Sb₂S₃ and its solar cell application, *Mater. Lett.* 233 (2018) 90–93.
- [30] W.H. Kim, S. Woo, K.-P. Kim, S.-M. Kwon, D.-H. Kim, Efficient TiO₂ surface treatment using Cs₂CO₃ for solution-processed planar-type Sb₂S₃ solar cells, *Nanoscale Res. Lett.* 14 (2019) 25.
- [31] C. Gao, J. Huang, H. Li, K. Sun, Y. Lai, M. Jia, L. Jiang, F. Liu, Fabrication of Sb₂S₃ thin films by sputtering and post-annealing for solar cells, *Ceram. Int.* 45 (2019) 3044–3051.
- [32] H. Lei, J. Chen, Z. Tan, G. Fang, Review of recent progress in antimony chalcogenide-based solar cells: materials and devices, *Solar RRL* 3 (2019), 1900026.
- [33] E. Kärber, A. Katerski, I. Oja Acik, A. Mere, V. Mikli, M. Krunk, Sb₂(S)₃ grown by ultrasonic spray pyrolysis and its application in a hybrid solar cell, *Beilstein J. Nanotechnol.* 7 (2016) 1662–1673.
- [34] M. Kriisa, M. Krunk, I. Oja Acik, E. Kärber, V. Mikli, The effect of tartaric acid in the deposition of Sb₂S₃ films by chemical spray pyrolysis, *Mater. Sci. Semicond. Process.* 40 (2015) 867–872.
- [35] J.S. Eensalu, A. Katerski, E. Kärber, I.O. Acik, A. Mere, M. Krunk, Uniform Sb₂S₃ optical coatings by chemical spray method, *Beilstein J. Nanotechnol.* 10 (2019) 198–210.
- [36] R.G. Avilez Garcia, C.A. Meza Avendaño, M. Pal, F. Paraguay Delgado, N.R. Mathews, Antimony sulfide (Sb₂S₃) thin films by pulse electrodeposition: effect of thermal treatment on structural, optical and electrical properties, *Mater. Sci. Semicond. Process.* 44 (2016) 91–100.
- [37] F. Aousgi, M. Kanzari, Structural and optical properties of amorphous Sb₂S₃ thin films deposited by vacuum thermal evaporation method, *Curr. Appl. Phys.* 13 (2013) 262–266.
- [38] N. Mahuli, D. Halder, A. Paul, S.K. Sarkar, Atomic layer deposition of amorphous antimony sulfide (a-Sb₂S₃) as semiconductor sensitizer in extremely thin absorber solar cell, *J. Vac. Sci. Technol.* 38 (2020), 032407.
- [39] E. Gil, S.-J. Lee, S.-J. Sung, K. Cho, D.-H. Kim, Spin-coating process of an inorganic Sb₂S₃ thin film for photovoltaic applications, *J. Nanosci. Nanotechnol.* 16 (2016) 10763–10766.
- [40] M. Barr, L. Assaud, Y. Wu, J. Bachmann, L. Santinacci, Atomic layer deposition of i-Sb₂S₃/p-NiO thin layers into anodic alumina membranes for photoelectrochemical water splitting, *ECS Trans.* 66 (2015) 119.
- [41] S. Sabnis, P.A. Bhadane, P.G. Kulkarni, Process flow of spray pyrolysis technique 4 (2013) 7–11.
- [42] V. Killedar, C. Lokhande, C. Bhosale, Preparation and characterization of spray deposited Sb₂S₃ thin films from non-aqueous medium, *Mater. Chem. Phys.* 47 (1997) 104–107.
- [43] E. Moustafa, J.G. Sanchez, L.F. Marsal, J. Pallarès, Stability enhancement of high-performance inverted polymer solar cells using ZnO electron interfacial layer deposited by intermittent spray pyrolysis, *Approach* 4 (2021) 4099–4111.
- [44] S.L. Hamukwaya, H. Hao, Z. Zhao, J. Dong, T. Zhong, J. Xing, L. Hao, M.M.J.C. Mashingaidze, A Review of Recent Developments in Preparation Methods for Large-Area Perovskite Solar Cells, vol. 12, 2022, p. 252.

- [45] A.M. Salem, M.S. Selim, A.M. Salem, Structure and optical properties of chemically deposited Sb₂S₃ thin films, *J. Phys. D Appl. Phys.* 34 (2000) 12–17.
- [46] F. Wu, R. Pathak, L. Jiang, W. Chen, C. Chen, Y. Tong, T. Zhang, R. Jian, Q. Qiao, Sb₂S₃ thickness-related photocurrent and optoelectronic processes in TiO₂/Sb₂S₃/P3HT planar hybrid solar cells, *Nanoscale Res. Lett.* 14 (2019) 325.
- [47] S. Yuan, H. Deng, X. Yang, C. Hu, J. Khan, W. Ye, J. Tang, H. Song, Postsurface selenization for high performance Sb₂S₃ planar thin film solar cells, *ACS Photonics* 4 (2017) 2862–2870.
- [48] J. Escorcia-García, E. Barrios-Salgado, M.T.S. Nair, P.K. Nair, Sb₂S₃/SnSe thin film solar cells by thermal evaporation, *MRS Proceedings* 1670 (2014) mrs14-1670-e1605-1610.
- [49] E. Gnenna, N. Khemiri, M. Kong, M.I. Alonso, M. Kanzari, Effect of Vacuum Annealing on the Properties of One Step Thermally Evaporated Sb₂S₃ Thin Films for Photovoltaic Applications, vol. 96, 2021, 20301.
- [50] Y. Osorio Mayon, T.P. White, R. Wang, Z. Yang, K.R. Catchpole, Evaporated and solution deposited planar Sb₂S₃ solar cells: a comparison and its significance, *Phys. Status Solidi* 213 (2016) 108–113.
- [51] J. Luo, W. Xiong, G. Liang, Y. Liu, H. Yang, Z. Zheng, X. Zhang, P. Fan, S. Chen, Fabrication of Sb₂S₃ thin films by magnetron sputtering and post-sulfurization/selenization for substrate structured solar cells, *J. Alloys Compd.* 826 (2020), 154235.
- [52] J. Han, S. Wang, J. Yang, S. Guo, Q. Cao, H. Tang, X. Pu, B. Gao, X. Li, Solution-processed Sb₂S₃ planar thin film solar cells with a conversion efficiency of 6.9% at an open circuit voltage of 0.7 V achieved via surface passivation by a SbCl₃ interface layer, *ACS Appl. Mater. Interfaces* 12 (2020) 4970–4979.
- [53] S.-J. Sung, E.K. Gil, S.-J. Lee, Y.C. Choi, K.-J. Yang, J.-K. Kang, K.Y. Cho, D.-H. Kim, Systematic control of nanostructured interfaces of planar Sb₂S₃ solar cells by simple spin-coating process and its effect on photovoltaic properties, *J. Ind. Eng. Chem.* 56 (2017) 196–202.
- [54] X. Wang, J. Li, W. Liu, S. Yang, C. Zhu, T. Chen, A fast chemical approach towards Sb₂S₃ film with a large grain size for high-performance planar heterojunction solar cells, *Nanoscale* 9 (2017) 3386–3390.
- [55] B. Roy, B.R. Chakraborty, R. Bhattacharya, A.K. Dutta, Electrical and magnetic properties of antimony sulphide (Sb₂S₃) crystals and the mechanism of carrier transport in it, *Solid State Commun.* 25 (1978) 937–940.
- [56] B. Peter, N. Werner, Refinement of the crystal structure of stibnite, Sb₂S₃, *Z. für Kristallogr. - Cryst. Mater.* 135 (1972) 308–315.
- [57] S. Scavnicar, The crystal structure of stibnite. A redetermination of atomic positions, *Z. Kristallogr.* 114 (1960) 5–9.
- [58] R. Tang, X. Wang, C. Jiang, S. Li, W. Liu, H. Ju, S. Yang, C. Zhu, T. Chen, n-Type doping of Sb₂S₃ light-harvesting films enabling high-efficiency planar heterojunction solar cells, *ACS Appl. Mater. Interfaces* 10 (2018) 30314–30321.
- [59] W. Lian, C. Jiang, Y. Yin, R. Tang, G. Li, L. Zhang, B. Che, T. Chen, Revealing composition and structure dependent deep-level defect in antimony trisulfide photovoltaics, *Nat. Commun.* 12 (2021) 3260.
- [60] A. Radzwan, R. Ahmed, A. Shaari, A. Lawal, Y.X. Ng, First-principles calculations of antimony sulphide Sb₂S₃, *Malaysian Journal of Fundamental and Applied Sciences* 13 (2017).
- [61] H. Koc, A.M. Mamedov, E. Deligoz, H. Ozisik, First principles prediction of the elastic, electronic, and optical properties of Sb₂S₃ and Sb₂Se₃ compounds, *Solid State Sci.* 14 (2012) 1211–1220.
- [62] B. Krishnan, A. Arato, E. Cardenas, T.K.D. Roy, G.A. Castillo, On the structure, morphology, and optical properties of chemical bath deposited Sb₂S₃ thin films, *Appl. Surf. Sci.* 254 (2008) 3200–3206.
- [63] R. Vadapoo, S. Krishnan, H. Yilmaz, C. Marin, Self-standing nanoribbons of antimony selenide and antimony sulfide with well-defined size and band gap, *Nanotechnology* 22 (2011), 175705.
- [64] M. Nair, Y. Pena, J. Campos, V. Garcia, P. Nair, Chemically deposited Sb₂S₃ and Sb₂S₃-CuS thin films, *J. Electrochem. Soc.* 145 (1998) 2113.
- [65] G. Murtaza, M. Akhtar, M.A. Malik, P. O'Brien, N. Revaprasadu, Aerosol assisted chemical vapor deposition of Sb₂S₃ thin films: environmentally benign solar energy material, *Mater. Sci. Semicond. Process.* 40 (2015) 643–649.
- [66] B. Nayak, H. Acharya, T. Chaudhuri, G. Mitra, The dip-dry technique for preparing photosensitive Sb₂S₃ films, *J. Thin Solid Films* 92 (1982) 309–314.
- [67] A. Ubale, V. Deshpande, Y. Shinde, D. Gulwade, Electrical, optical and structural properties of nanostructured Sb₂S₃ thin films deposited by CBD technique, *J. Chalcogenide Letters* 7 (2010) 101–109.
- [68] P. Büttner, F. Scheler, C. Pointer, D. Döhler, M.K.S. Barr, A. Koroleva, D. Pankin, R. Hatada, S. Flege, A. Manshina, E.R. Young, I. Mínguez-Bacho, J. Bachmann, Adjusting interfacial Chemistry and electronic properties of photovoltaics based on a highly pure Sb₂S₃ absorber by atomic layer deposition, *ACS Appl. Energy Mater.* 2 (2019) 8747–8756.
- [69] P. Büttner, D. Döhler, S. Korenko, S. Möhrlein, S. Bochmann, N. Vogel, I. Mínguez-Bacho, J. Bachmann, Solid state interdigitated Sb₂S₃ based TiO₂ nanotube solar cells, *RSC Adv.* 10 (2020) 28225–28231.
- [70] J.A. Chang, J.H. Rhee, S.H. Im, Y.H. Lee, H.-j. Kim, S.I. Seok, M.K. Nazeeruddin, M. Grätzel, High-performance nanostructured Inorganic–Organic heterojunction solar cells, *Nano Lett.* 10 (2010) 2609–2612.
- [71] J.C. Cardoso, C.A. Grimes, X. Feng, X. Zhang, S. Komarneni, M.V.B. Zanoni, N. Bao, Fabrication of coaxial TiO₂/Sb₂S₃ nanowire hybrids for efficient nanostructured organic–inorganic thin film photovoltaics, *Chem. Commun.* 48 (2012) 2818–2820.
- [72] T. Fukumoto, T. Moehl, Y. Niwa, M.K. Nazeeruddin, M. Grätzel, L. Etgar, Effect of interfacial engineering in solid-state nanostructured Sb₂S₃ heterojunction solar cells, *Adv. Energy Mater.* 3 (2013) 29–33.
- [73] S. Ito, K. Tsujimoto, D.-C. Nguyen, K. Manabe, H. Nishino, Doping effects in Sb₂S₃ absorber for full-inorganic printed solar cells with 5.7% conversion efficiency, *Int. J. Hydrogen Energy* 38 (2013) 16749–16754.
- [74] K.C. Gödel, B. Roose, A. Sadhanala, Y. Vaynzof, S.K. Pathak, U. Steiner, Partial oxidation of the absorber layer reduces charge carrier recombination in antimony sulfide solar cells, *Phys. Chem. Chem. Phys.* 19 (2017) 1425–1430.
- [75] H. Sabit, S. Omer, Synthesis, characterization and photovoltaic properties of Mn-doped Sb₂S₃ thin film, *Materials Science-Poland* 35 (2017) 861–867.
- [76] S. Horoz, K. Hüsnü, Ö. Şahin, Investigation of structural, optical and photovoltaic properties of Sb₂S₃ thin films, *J. Cumhuriyet Sci.* 38 (2017) 588–593.
- [77] Q. Ye, Y. Xu, W. Chen, S. Yang, J. Zhu, J. Weng, Enhanced photovoltaic performance of Sb₂S₃-sensitized solar cells through surface treatments, *Appl. Surf. Sci.* 440 (2018) 294–299.
- [78] M.S. You, C.-S. Lim, D.H. Kwon, J.H. Heo, S.H. Im, K.J. Chae, Oxide-free Sb₂S₃ sensitized solar cells fabricated by spin and heat-treatment of Sb (III)-thioacetamide) 2Cl₃, *Org. Electron.* 21 (2015) 155–159.
- [79] Y.C. Choi, S.I. Seok, Efficient Sb₂S₃-sensitized solar cells via single-step deposition of Sb₂S₃ using S/Sb-Ratio-Controlled SbCl₃-thiourea complex solution, *Adv. Funct. Mater.* 25 (2015) 2892–2898.
- [80] L. Zheng, K. Jiang, J. Huang, Y. Zhang, B. Bao, X. Zhou, H. Wang, B. Guan, L.M. Yang, Y. Song, Solid-state nanocrystalline solar cells with an antimony sulfide absorber deposited by an in situ solid–gas reaction, *J. Mater. Chem.* 5 (2017) 4791–4796.
- [81] L. Zhang, C. Wu, W. Liu, S. Yang, M. Wang, T. Chen, C. Zhu, Sequential deposition route to efficient Sb₂S₃ solar cells, *J. Mater. Chem.* 6 (2018) 21320–21326.
- [82] C. Jiang, R. Tang, X. Wang, H. Ju, G. Chen, T. Chen, Alkali metals doping for high-performance planar heterojunction Sb₂S₃ solar cells, *Solar RRL* 3 (2019), 1800272.
- [83] R. Tang, X. Wang, C. Jiang, S. Li, G. Jiang, S. Yang, C. Zhu, T. Chen, Vacuum assisted solution processing for highly efficient Sb₂S₃ solar cells, *J. Mater. Chem.* 6 (2018) 16322–16327.
- [84] C. Guo, J. Chen, G. Li, X. Liang, W. Lai, L. Yang, Y. Mai, Z. Li, Enhanced Electrical Conductivity of Sb₂S₃ Thin Film via C60 Modification and Improvement in Solar Cell Efficiency, *Glob. Chall.* 2019, 1800108.
- [85] M. Tamilselvan, A. Byregowda, C.-Y. Su, C.-J. Tseng, A.J. Bhattacharyya, Planar heterojunction solar cell employing a single-source precursor solution-processed Sb₂S₃ thin film as the light absorber, *ACS Omega* 4 (2019) 11380–11387.
- [86] A. Maiti, S. Chatterjee, A.J. Pal, Sulfur-vacancy passivation in solution-processed Sb₂S₃ thin films: influence on photovoltaic interfaces, *ACS Appl. Energy Mater.* 3 (2019) 810–821.
- [87] Y. Zeng, K. Sun, J. Huang, M.P. Nielsen, F. Ji, C. Sha, S. Yuan, X. Zhang, C. Yan, X. Liu, Quasi-vertically-orientated antimony sulfide inorganic thin-film solar cells achieved by vapor transport deposition, *ACS Appl. Mater. Interfaces* 12 (2020) 22825–22834.
- [88] E.M. Mkawi, Solvothermal orthorhombic Sb₂S₃ nanobars: effect of hydrothermal temperature in properties for solar cell application, *Results Phys.* 19 (2020), 103603.
- [89] X. Jin, Y. Fang, T. Salim, M. Feng, S. Hadke, S.W. Leow, T.C. Sum, L.H. Wong, In situ growth of [hk1]-Oriented Sb₂S₃ for solution-processed planar heterojunction solar cell with 6.4% efficiency, *Adv. Funct. Mater.* 30 (2020), 2002887.
- [90] H. Lei, T. Lin, X. Wang, P. Dai, Y. Guo, Y. Gao, D. Hou, J. Chen, Z. Tan, Copper doping of Sb₂S₃: fabrication, properties, and photovoltaic application, *J. Mater. Sci. Mater. Electron.: Materials in Electronics* 30 (2019) 21106–21116.
- [91] J.S. Eensalu, A. Katerski, E. Kärber, L. Weinhardt, M. Blum, C. Heske, W. Yang, I.O. Acik, M. Krunk, Semitransparent Sb₂S₃ thin film solar cells by ultrasonic spray pyrolysis for use in solar windows, *Beilstein J. Nanotechnol.* 10 (2019) 2396–2409.
- [92] A.M. Huerta-Flores, N.A. García-Gómez, S.M. De la Parra-Arciniegua, E.M. Sánchez, Technology, Fabrication and characterization of a nanostructured TiO₂/In₂S₃-Sb₂S₃/CuSCN extremely thin absorber (eta) solar cell, *J. Semicond. Sci.* 31 (2016), 085011.
- [93] E. Mkawi, R. Almallki, Y. Al-Hadeethi, Influence of different concentrations of SbCl₃ salt on the properties of Sb₂S₃ nanobars prepared by the solvothermal method for solar cell application, *J. Opt. Mater. Express* 11 (2021) 2219–2233.
- [94] J. Escorcia-García, D. Becerra, M.T.S. Nair, P.K. Nair, Heterojunction CdS/Sb₂S₃ solar cells using antimony sulfide thin films prepared by thermal evaporation, *Thin Solid Films* 569 (2014) 28–34.
- [95] S. Yuan, H. Deng, D. Dong, X. Yang, K. Qiao, C. Hu, H. Song, H. Song, Z. He, J. Tang, Efficient planar antimony sulfide thin film photovoltaics with large grain and preferential growth, *Sol. Energy Mater. Sol. Cells* 157 (2016) 887–893.
- [96] X. Chen, Z. Li, H. Zhu, Y. Wang, B. Liang, J. Chen, Y. Xu, Y. Mai, CdS/Sb₂S₃ heterojunction thin film solar cells with a thermally evaporated absorber, *J. Mater. Chem. C* 5 (2017) 9421–9428.
- [97] S. Qiao, J. Liu, Z. Li, S. Wang, G. Fu, Sb₂S₃ thickness-dependent lateral photovoltaic effect and time response observed in glass/FTO/CdS/Sb₂S₃/Au structure, *J. Opt. Express* 25 (2017) 19583–19594.

- [98] K. Wang, J. Cheng, X. Yang, R. Hu, L. Fu, J. Huang, J. Yu, L. Li, Enhanced photovoltaic properties in Sb₂S₃ planar heterojunction solar cell with a fast selenylation approach, *Nanoscale Res. Lett.* 13 (2018).
- [99] G. Pan, D. Wang, S. Gao, P. Gao, Q. Sun, X. Liu, Z. Zhou, Y. Sun, Y. Zhang, Substrate structured Sb₂S₃ thin film solar cells fabricated by rapid thermal evaporation method, *J. Sol. Energy* 182 (2019) 64–71.
- [100] Y. Yin, C. Wu, R. Tang, C. Jiang, G. Jiang, W. Liu, T. Chen, C. Zhu, Composition engineering of Sb₂S₃ film enabling high performance solar cells, *Sci. Bull.* 64 (2019) 136–141.
- [101] K.C. Mandal, A. Mondal, A new chemical method for preparing semiconductor grade antimony tri-sulphide thin films, *J. Phys. Chem. Solid.* 51 (1990) 1339–1341.
- [102] O. Savadogo, K. Mandal, Characterizations of antimony tri-sulfide chemically deposited with silicotungstic acid, *J. Electrochem. Soc.* 139 (1992) L16.
- [103] C. Lokhande, Chemical deposition of metal chalcogenide thin films, *Mater. Chem. Phys.* 27 (1991) 1–43.
- [104] K.C. Gödel, Y.C. Choi, B. Roose, A. Sadhanala, H.J. Snaith, S.I. Seok, U. Steiner, S.K. Pathak, Efficient room temperature aqueous Sb₂S₃ synthesis for inorganic–organic sensitized solar cells with 5.1% efficiencies, *J. Chem. Commun.* 51 (2015) 8640–8643.
- [105] N. Maiti, S.H. Im, C.-S. Lim, S.I. Seok, A chemical precursor for depositing Sb₂S₃ onto mesoporous TiO₂ layers in nonaqueous media and its application to solar cells, *Dalton Trans.* 41 (2012) 11569–11572.
- [106] M. Nair, Y. Peña, J. Campos, V. García, P. Nair, Chemically deposited Sb₂S₃ and Sb₂S₃-CuS thin films, *J. Electrochem. Soc.* 145 (1998) 2113–2120.
- [107] S. Srikanth, N. Suriyanarayanan, S. Prabakar, V. Balasubramanian, D. Kathirvel, Structural and optical properties of chemical bath deposited Sb₂S₃ thin films, *Adv. Sci. Res.* 2 (2011) 95–104.
- [108] Z. Xiaoping, L. Zhang, W. Jihuai, L. Jianming, F. Leqing, Enhancing photovoltaic performance of photoelectrochemical solar cells with nano-sized ultra thin Sb₂S₃-sensitized layers in photoactive electrodes, *J. Mater. Sci. Mater. Electron.: Materials in Electronics* 24 (2013) 1970–1975.
- [109] J.A. Chang, S.H. Im, Y.H. Lee, H.-j. Kim, C.-S. Lim, J.H. Heo, S.I. Seok, Panchromatic photon-harvesting by hole-conducting materials in inorganic–organic heterojunction sensitized-solar cell through the formation of nanostructured electron channels, *Nano Lett.* 12 (2012) 1863–1867.
- [110] Z. Chen, G. Chen, The effect of absorber thickness on the planar Sb₂S₃ thin film solar cell: trade-off between light absorption and charge separation, *Sol. Energy* 201 (2020) 323–329.
- [111] V.A. Patil, A.R. Patil, J.W. Choi, D.S. Paik, S.J. Yoon, Preparation and characterization of chemically deposited mixed (Bi_{1-x}Sb_x)₂S₃ thin films, *Surf. Eng.* 23 (2007) 28–31.
- [112] M. Shang, J. Zhang, S. Wei, Y. Zhu, L. Wang, H. Hou, T. Fujikawa, N. Ueno, Y. Wu, Bi doped Sb₂S₃ for low effective mass and optimized optical property, *J. Mater. Chem. C* 4 (2016) 5081–5090.
- [113] M. Kamruzzaman, L. Chaoping, F. Yishu, A.F.U. Islam, J. Zapien, Atmospheric annealing effect on TiO₂/Sb₂S₃/P3HT heterojunction hybrid solar cell performance, *RSC Adv.* 6 (2016) 99282–99290.
- [114] D.U. Lee, S.W. Pak, S.G. Cho, E.K. Kim, S.I. Seok, Defect states in hybrid solar cells consisting of Sb₂S₃ quantum dots and TiO₂ nanoparticles, *Appl. Phys. Lett.* 103 (2013), 023901.
- [115] H.-W. Kang, J.-W. Lee, N.-G. Park, Effect of double blocking layers at TiO₂/Sb₂S₃ and Sb₂S₃/Spiro-MeOTAD interfaces on photovoltaic performance, *Faraday Discuss* 176 (2014) 287–299.
- [116] Y. Xu, W. Chen, X. Ding, X. Pan, L. Hu, S. Yang, J. Zhu, S. Dai, An ultrathin SiO₂ blocking layer to suppress interfacial recombination for efficient Sb₂S₃-sensitized solar cells, *Inorg. Chem. Front.* 5 (2018) 1370–1377.
- [117] H. Lei, G. Yang, Y. Guo, L. Xiong, P. Qin, X. Dai, X. Zheng, W. Ke, H. Tao, Z. Chen, B. Li, G. Fang, Efficient planar Sb₂S₃ solar cells using a low-temperature solution-processed tin oxide electron conductor, *Phys. Chem. Chem. Phys.* 18 (2016) 16436–16443.
- [118] Y. Itzhaik, O. Niitsoo, M. Page, G. Hodes, Sb₂S₃-Sensitized nanoporous TiO₂ solar cells, *J. Phys. Chem. C* 113 (2009) 4254–4256.
- [119] Y.C. Choi, S.I. Seok, Efficient Sb₂S₃-sensitized solar cells via single-step deposition of Sb₂S₃ using S/Sb-Ratio-Controlled SbCl₃-thiourea complex solution 25, 2015, pp. 2892–2898.
- [120] X. Jin, Y. Yuan, C. Jiang, H. Ju, G. Jiang, W. Liu, C. Zhu, T. Chen, Solution processed NiOx hole-transporting material for all-inorganic planar heterojunction Sb₂S₃ solar cells, *Sol. Energy Mater. Sol. Cells* 185 (2018) 542–548.
- [121] H. Zhou, J. Han, X. Pu, X. Li, Effective additive for enhancing the performance of Sb₂S₃ planar thin film solar cells, *J. Materiomics* 7 (2021) 1074–1082.
- [122] J. Han, X. Pu, H. Zhou, Q. Cao, S. Wang, J. Yang, J. Zhao, X. Li, Multidentate anchoring through additive engineering for highly efficient Sb₂S₃ planar thin film solar cells, *J. Mater. Sci. Technol.* 89 (2021) 36–44.
- [123] P. Kaenaburg, B. Klingebiel, T. Kirchartz, Spin-coated planar Sb₂S₃ hybrid solar cells approaching 5% efficiency, *Beilstein J. Nanotechnol.* 9 (2018) 2114–2124.
- [124] Y. Li, Y. Wei, K. Feng, Y. Hao, J. Pei, B. Sun, Preparation of Sb₂S₃ nanocrystals modified TiO₂ dendritic structure with nanotubes for hybrid solar cell, *Mater. Res. Express* 5 (2018), 065903.
- [125] J. Chen, J. Qi, R. Liu, X. Zhu, Z. Wan, Q. Zhao, S. Tao, C. Dong, G.Y. Ashebir, W. Chen, R. Peng, F. Zhang, S. Yang, X. Tian, M. Wang, Preferentially oriented large antimony trisulfide single-crystalline cuboids grown on polycrystalline titania film for solar cells, *Commun. Chem.* 2 (2019) 121.
- [126] R. Liu, Z. Shen, Z. Wan, L. Zhu, J. Chen, C. Dong, W. Chen, W. Cao, B. Chen, X. Yuan, Nanoarray heterojunction and its efficient solar cells without negative impact of photogenerated electric field, *J. Commun. Phys.* 4 (2021) 1–12.
- [127] C.H. Bhosale, M.D. Uplane, P.S. Patil, C.D. Lockhande, Preparation and properties of sprayed antimony trisulphide films, *Thin Solid Films* 248 (1994) 137–139.
- [128] K.Y. Rajpure, C.H. Bhosale, Preparation and characterization of spray deposited photoactive Sb₂S₃ and Sb₂Se₃ thin films using aqueous and non-aqueous media, *Mater. Chem. Phys.* 73 (2002) 6–12.
- [129] J.S. Eensalu, A. Katerski, E. Kärber, I. Oja Acik, A. Mere, M. Krunk, Uniform Sb₂S₃ optical coatings by chemical spray method, *Beilstein J. Nanotechnol.* (2019) 198–210.
- [130] G. Hector, J.S. Eensalu, A. Katerski, H. Roussel, O. Chaix-Pluchery, E. Appert, F. Donatini, I.O. Acik, E. Kärber, V. Consonni, Optimization of the Sb₂S₃ shell thickness in ZnO nanowire-based extremely thin absorber solar cells, *Nanomaterials* 12 (2022) 198.
- [131] R. Parize, T. Cossuet, E. Appert, O. Chaix-Pluchery, H. Roussel, L. Rapenne, V. Consonni, Synthesis and properties of ZnO/TiO₂/Sb₂S₃ core-shell nanowire heterostructures using the SILAR technique, *CrystEngComm* 20 (2018) 4455–4462.
- [132] S.-M. Yoo, J.-Y. Oh, H.J. Lee, Quantum dot-sensitizers prepared by SILAR and cation-exchange processes, *J. Kor. Chem. Soc.* 62 (2018) 341–343.
- [133] H. Zhang, L. Song, L. Luo, L. Liu, H. Wang, F. Wang, TiO₂/Sb₂S₃/P3HT based inorganic–organic hybrid heterojunction solar cells with enhanced photoelectric conversion performance, *J. Electron. Mater.* 46 (2017) 4670–4675.
- [134] R. Parize, A. Katerski, I. Gromyko, L. Rapenne, H. Roussel, E. Kärber, E. Appert, M. Krunk, V. Consonni, ZnO/TiO₂/Sb₂S₃ core-shell nanowire heterostructure for extremely thin absorber solar cells, *J. Phys. Chem. C* 121 (2017) 9672–9680.
- [135] T.S. Senthil, N. Muthukumarasamy, M. Kang, Study of various Sb₂S₃ nanostructures synthesized by simple solvothermal and hydrothermal methods, *Mater. Char.* 95 (2014) 164–170.
- [136] J. Kavinchan, T. Thongtem, S. Thongtem, E. Saksornchai, Synthesis of coral-like, straw-like, and flower-like antimony sulfides by a facile wet-chemical method, *J. Journal of Nanomaterials* (2013) 2013.
- [137] M. Abulikemu, S. Del Gobbo, D.H. Anjum, M.A. Malik, O.M. Bakr, Colloidal Sb₂S₃ nanocrystals: synthesis, characterization and fabrication of solid-state semiconductor sensitized solar cells, *J. Mater. Chem. A* 4 (2016) 6809–6814.
- [138] J. Ota, P. Roy, S.K. Srivastava, B.B. Nayak, A.K. Saxena, Morphology evolution of Sb₂S₃ under hydrothermal conditions: flowerlike structure to nanorods, *Cryst. Growth Des.* 8 (2008) 2019–2023.
- [139] M. Pal, N.R. Mathews, X. Mathew, Surfactant-mediated self-assembly of Sb₂S₃ nanorods during hydrothermal synthesis, *J. Mater. Res.* 32 (2017) 530–538.
- [140] M. Liu, Y. Gong, Z. Li, M. Dou, F. Wang, A green and facile hydrothermal approach for the synthesis of high-quality semi-conducting Sb₂S₃ thin films, *J. Appl. Surf. Sci.* 387 (2016) 790–795.
- [141] O.A. Jaramillo-Quintero, A. Baron-Jaimes, R.A. Miranda-Gamboa, M.E. Rincon, Cadmium-free ZnS interfacial layer for hydrothermally processed Sb₂S₃ solar cells, *Sol. Energy* 224 (2021) 697–702.
- [142] J.R. Castro, K.C. Molloy, Y. Liu, C.S. Lai, Z. Dong, T.J. White, E.R.T. Tiekink, Formation of antimony sulfide powders and thin films from single-source antimony precursors, *J. Mater. Chem.* 18 (2008) 5399–5405.
- [143] H. Deng, Y. Zeng, M. Ishaq, S. Yuan, H. Zhang, X. Yang, M. Hou, U. Farooq, J. Huang, K. Sun, R. Webster, H. Wu, Z. Chen, F. Yi, H. Song, X. Hao, J. Tang, Quasipitaxy strategy for efficient full-inorganic Sb₂S₃ solar cells, *Adv. Funct. Mater.* 29 (2019), 1901720.
- [144] M. Ishaq, S. Chen, U. Farooq, M. Azam, H. Deng, Z.-H. Su, Z.-H. Zheng, P. Fan, H.-S. Song, G.-X. Liang, High open-circuit voltage in full-inorganic Sb₂S₃ solar cell via modified Zn-doped TiO₂ electron transport layer, *Sol. RRL* 4 (2020), 2000551.
- [145] Y. Zeng, F. Liu, X. Hao, Fabrication of Sb₂S₃ planar thin film solar cells with closed-space sublimation method, in: IEEE 7th World Conference on Photovoltaic Energy Conversion (WCPEC) (A Joint Conference of 45th IEEE PVSEC & 28th PVSEC & 34th EU PVSEC), 2018, 2018, pp. 870–872.
- [146] L. Guo, B. Zhang, S. Li, Q. Zhang, M. Buettner, L. Li, X. Qian, F. Yan, Scalable and efficient Sb₂S₃ thin-film solar cells fabricated by close space sublimation, *Appl. Mater.* 7 (2019), 041105.